Phosphate budgeting to mitochondria controls glucose-mediated mitochondrial repression

Vineeth Vengayil[1,2], Shreyas Niphadkar[1,2], Swagata Adhikary[1,2], Sriram Varahan[1], Sunil Laxman[1]*

1. Institute for Stem Cell Science and Regenerative Medicine (DBT-inStem)
   GKVK Post Bellary Road
   Bangalore 560065
2. Manipal Academy of Higher Education, Manipal, Karnataka 576104, India

*correspondence: sunil@instem.res.in

Keywords: mitochondria, glycolysis, phosphate, deubiquitinase, Crabtree, Warburg, Usp10, Ubp3

Abstract

Many cells growing in high glucose repress mitochondrial respiration, as observed in the Crabtree and Warburg effects. A parsimonious biochemical explanation for this phenomenon is missing. Using a *Saccharomyces cerevisiae* screen, we identified the conserved deubiquitinase Ubp3 (Usp10), as necessary for proper mitochondrial repression. Ubp3 mutants have increased mitochondrial activity despite abundant glucose, with downregulated glycolytic enzymes, rewired glucose metabolism, and increased trehalose. Utilizing *Δubp3* cells, along with orthogonal approaches, we find that the Crabtree effect is driven mechanistically by controling mitochondrial access of inorganic phosphate (Pi), as determined by glycolytic flux. High glycolytic flux consumes free Pi, limiting available Pi for entry into the mitochondria. Cytosolic Pi-dependent mitochondrial Pi entry is necessary and sufficient to derepress mitochondria, driving synchronous requirements to sustain mitochondrial activity. Restricting Pi entry to the mitochondria prevents mitochondrial derepression. Collectively, we propose a biochemical basis of mitochondrial repression in high-glucose based on intracellular Pi budgeting.

Introduction

Rapidly proliferating cells have substantial metabolic and energy demands, which are required in order to increase biomass (Buchakjian & Kornbluth, 2010; Cai & Tu, 2011; Zhu & Thompson, 2019). This includes a high ATP demand, obtained from cytosolic glycolysis or mitochondrial oxidative phosphorylation (OXPHOS), to fuel multiple reactions (Nelson et al., 2008). Interestingly, many rapidly proliferating cells have reduced mitochondrial respiration in high glucose. These cells preferentially rely on ATP generated from glycolysis/fermentation over mitochondrial respiration and OXPHOS, even though the net ATP yield per glucose molecule from glycolysis is lower than OXPHOS (López-lázaro, 2008). This occurs even in oxygen replete conditions, and is the well-known Warburg effect (Heiden et al., 2009; Warburg, 1925). A feature of many of these cells is the repression of mitochondrial processes in high glucose, termed glucose-mediated mitochondrial repression or simply the Crabtree effect (Crabtree, 1929; De Deken, 1966). This phenomenon is observed in many cells including some tumors (Heiden et al., 2009), neutrophils (Xia et al., 2021), activated macrophages (Kornberg, 2020), stem cells (Abdel-Haleem et al., 2017; Pacini & Borziani, 2014; Tsogtbaatar et al., 2020), and most famously *S. cerevisiae* (De Deken, 1966). Understanding how such cells growing in high glucose repress their mitochondria is therefore of obvious interest to diverse researchers. Numerous studies have identified signaling programs or regulators involved in glucose mediated mitochondrial repression. However, biochemical programs and regulatory processes in biology typically evolve around key biochemical constraints (Cornish-Bowden, 2016). The minimal biochemical constraints that explain how this phenomenon occurs are unresolved (Diaz-Ruiz et al., 2011; Hammad et al., 2016).

There are two major still unresolved hypotheses on the biochemical origins of the Crabtree effect. The first proposes direct roles for glycolytic intermediates in regulating mitochondrial respiration, by inhibiting specific mitochondrial outputs (Díaz-Ruiz et al., 2008; Lemus et al., 2018). The second proposes that cytosolic and mitochondrial processes compete for a common substrate. For example, a balance between pyruvate utilization in fermentation vs the mitochondrial TCA cycle (mediated by mitochondrial pyruvate transport and the pyruvate dehydrogenase complex) could determine mitochondrial activity under high glucose (Diaz-Ruiz et al., 2011). Relatedly, a competition between glycolytic and mitochondrial processes for mutually required metabolites/co-factors such as ADP or inorganic phosphate (Pi) could also regulate mitochondrial activity (Diaz-Ruiz et al., 2011; Hammad et al., 2016;

64 Koobs, 1972). This second hypothesis therefore proposes that an imbalance in resource
65 allocations within the cell might limit access of these metabolites to the mitochondria, causing
66 mitochondrial repression. These are not all mutually exclusive, and a combination of these
67 factors might dictate mitochondrial repression in high glucose. However, any hierarchies of
68 importance are currently unclear (Rodríguez-Enríquez et al., 2001). Collectively, experimental
69 data for a biochemical basis to explain mitochondrial repression remains incomplete.

70 One approach to resolve this question has been to identify regulators of metabolic
71 state under high glucose. Mitochondrial repression occurs rapidly after glucose addition
72 (Bouchez et al., 2020), and post-translational modifications regulated by signaling systems
73 might regulate this process (Broach, 2012; Hitosugi & Chen, 2014; Tripodi et al., 2015).
74 Ubiquitination is a major post-translational modification that regulates global proteostasis
75 (Hershko & Ciechanover, 1998; Komander & Rape, 2012), but the roles of ubiquitination-
76 dependent processes in regulating mitochondrial repression are poorly explored.
77 Ubiquitination itself is determined by the balance between E3-ligase dependent
78 ubiquitination, and deubiquitinase (DUB) dependent deubiquitination (Hershko et al., 1983;
79 Pickart & Eddins, 2004). Little is known about the roles of DUBs in regulating metabolic states,
80 making the DUBs interesting candidate regulators of mitochondrial repression.

81 In this study, using an *S. cerevisiae* DUB knock-out library based screen, we identified
82 the evolutionarily conserved Ubp3 protein (Usp10 in mammals) as required for mitochondrial
83 repression in high glucose. The loss of Ubp3 resulted in mitochondrial activation, and a
84 reduction in the glycolytic enzymes-phosphofructokinase 1 (Pfk1) and GAPDH isozymes Tdh1
85 and Tdh2, resulting in decreased glycolytic flux. The consequent rerouting of glucose flux also
86 increases trehalose biosynthesis. This metabolic rewiring alters the intracellular inorganic
87 phosphate (Pi) balance, due to both the increased Pi release from trehalose synthesis, and
88 decreased Pi consumption in glycolysis, to cumulatively increase Pi pools. Using *ubp3Δ* cells
89 along with independent analysis of wild-type cells, as well as isolated mitochondrial fractions
90 from these cells, we established that changing intracellular Pi budgeting via this metabolic
91 rewiring, and consequently increasing Pi allocations to mitochondria is necessary and
92 sufficient to increase mitochondrial activity. Switching to a respiratory state requires
93 increased mitochondrial Pi transport, and mitochondrial Pi regulates mitochondrial activity.
94 Through these data, we propose how intracellular Pi balance, and a cytosolic vs mitochondrial

95 competition for Pi as controlled by glycolytic flux, is a biochemical basis for the Crabtree
96 effect.

97 **Results**

98 **A deubiquitinase deletion screen identifies Ubp3 as a regulator of glucose-mediated**
99 **mitochondrial repression**

100 In Crabtree positive cells such as *Saccharomyces cerevisiae*, high glucose represses
101 mitochondrial activity as well as OXPHOS-dependent ATP synthesis (De Deken, 1966; Postma
102 et al., 1989) (illustrated in Figure 1A). Our initial objective was only to identify proteostasis
103 regulators of glucose-mediated mitochondrial repression. We generated and used a
104 deubiquitinase (DUB) deletion strain library of *S. cerevisiae* (Figure S1A), to unbiasedly screen
105 for putative regulators of mitochondrial repression (Figure 1B). For the screen, mitochondrial
106 activity in wild-type (WT) and mutant cells growing in 2% glucose were assessed based on the
107 fluorescence intensity of a potentiometric dye Mitotracker CMXRos (which measures the
108 mitochondrial membrane potential) (illustrated in Figure 1B). Using this screen, we identified
109 DUB mutants with altered mitochondrial membrane potential (Figure 1C, Figure S1A). Note:
110 WT cells in a respiratory medium (2% ethanol) were used as an added control to estimate
111 maximum mitotracker fluorescence intensity (Figure S1B).

112 A prominent 'hit' was the evolutionarily conserved deubiquitinase Ubp3 (Figure 1C),
113 which is the homolog of the mammalian deubiquitinase Usp10 (Figure S1C). This protein
114 shows a degree of conservation across eukaryotes (Figure S1C). Due to this reason, as well as
115 putative roles in metabolism or mitochondrial function (Isasa et al., 2015; Nostramo et al.,
116 2016; Ossareh-Nazari et al., 2010), we focused our further attention on this DUB. Cells lacking
117 Ubp3 showed an ~1.5-fold increase in mitotracker fluorescence (Figure 1C, Figure S1A). To
118 assess if the increased mitochondrial potential depends on the deubiquitinase activity of
119 Ubp3, we generated a catalytically dead mutant of Ubp3 - Ubp3^{C469A} and estimated
120 mitotracker fluorescence. Ubp3^{C469A} cells showed increased mitochondrial potential
121 comparable to *ubp3Δ* cells (Figure 1D). This data confirmed that the catalytic activity of Ubp3
122 is required to fully repress mitochondrial activity under high glucose. As a control, we also

123 assessed steady-state levels of Ubp3 protein (Figure S1D). The mutation in the catalytic site
124 did not affect steady-state Ubp3 levels.

125 Next, to assess the requirement of Ubp3 for mitochondrial function, we quantified the
126 electron transport chain (ETC) complex IV subunit Cox2 (Fontanesi et al., 2006)(Figure 1E).
127 *ubp3Δ* cells have significantly higher Cox2 protein than WT cells (Figure 1E). There was no
128 increase in the protein levels of mitochondrial outer membrane protein Tom70 (Figure S1E),
129 suggesting that the increased Cox2 is not merely because of an increase in total mitochondrial
130 content. We next measured the basal oxygen consumption rate (OCR) of *ubp3Δ* cells using
131 Seahorse XFe24 Analyzer. Notably, basal OCR is significantly higher in *ubp3Δ* cells, indicating
132 higher respiration (Figure 1F).

133 Since *ubp3Δ* cells have increased respiration, we asked if ATP synthesis from
134 mitochondria was higher in these cells. To estimate this, we measured total ATP levels in WT
135 and *ubp3Δ* cells, in the presence and absence of mitochondrial ETC complex IV inhibitor
136 sodium azide (Yoshikawa et al., 1998). This would quantify the contribution of mitochondrial
137 ETC dependent ATP synthesis to the total ATP pools (which come from both glycolysis and
138 respiration). The total ATP levels in WT and *ubp3Δ* cells were comparable (Figure 1G).
139 However, upon treatment with sodium azide, ATP levels in WT cells were significantly higher
140 than *ubp3Δ* cells, contributing to ~60% of the total ATP in these cells (Figure 1H). In contrast,
141 the ATP levels in *ubp3Δ* cells after sodium azide treatment were ~ 40% of the total ATP levels
142 (Figure 1H). These data suggest a higher contribution of mitochondrial ATP synthesis towards
143 the total ATP pool in *ubp3Δ* cells, as compared to WT cells.

144 We next asked if *ubp3Δ* cells required this high mitochondrial activity for growth. For
145 this, we first assessed growth in high glucose, in the presence and absence of sodium azide.
146 In high glucose, WT cells expectedly show a minimal growth defect in the presence of sodium
147 azide, indicating a low reliance on mitochondrial function (Figure 1I). Contrastingly, *ubp3Δ*
148 cells as well as Ubp3^{C469A} cells show a severe growth defect in the presence of sodium azide
149 (Figure 1I). Next, we reduced mitochondrial respiration by individually deleting several
150 components of the ETC (Cox2, and the ATP synthase subunits Atp1 and Atp10), and assessed
151 growth in WT and *ubp3Δ* cells. Loss of these genes results in a severe growth defect in *ubp3Δ*

152 cells as compared to in WT cells (Figure S1F). Together, these results indicate that the loss of
153 Ubp3 makes cells dependent on mitochondrial ATP synthesis in high glucose.

154 Collectively these data show that in 2% glucose, *ubp3Δ* cells have high mitochondrial
155 activity and respiration, and rely on this mitochondrial function for ATP production and
156 growth. We therefore decided to use *ubp3Δ* cells in order to delineate necessary
157 requirements for glucose-mediated mitochondrial repression.

158

159 **Key glycolytic enzymes decrease and glucose flux is rerouted in *ubp3Δ* cells**

160 Glucose-6 phosphate (G6P) is the central node in glucose metabolism where carbon-
161 allocations are made towards distinct metabolic arms, primarily: glycolysis, the pentose
162 phosphate pathway (PPP), and trehalose biosynthesis (Figure 2A). High glycolytic enzymes
163 ensure maximum glycolytic flux when sufficient glucose is present (Grigaitis & Teusink, 2022).
164 We first investigated what happens to glycolytic enzyme amounts in *ubp3Δ* cells. The
165 endogenous protein amounts of key glycolytic enzymes - Phosphofructokinase 1 (Pfk1),
166 GAPDH isozymes (Tdh2, Tdh3), and the enolase isozymes (Eno1, Eno2) were all compared
167 between WT and *ubp3Δ* cells. Pfk1, Tdh2, and Tdh3 proteins were significantly decreased in
168 *ubp3Δ* cells (but not Eno1 and Eno2) (Figure 2B, S2A). This observation was intriguing, because
169 the Pfk and GAPDH steps are critical in determining glycolytic flux. Pfk1 converts fructose 6-
170 phosphate (F6P) to fructose 1,6 bisphosphate (F1,6BP), a committed step of glycolysis (Nelson
171 et al., 2008). GAPDH converts glyceraldehyde 3-phosphate (G3P) to 1,3 bisphosphoglycerate
172 (1,3BPG), which is the major flux regulating step in the lower arm of glycolysis (Nelson et al.,
173 2008; Shestov et al., 2014) (Figure 2A). A reduction in these enzymes could therefore
174 putatively decrease glycolytic flux, and a subsequent reduction in the glycolytic rate could
175 reroute glucose (G6P) allocations via mass action towards other branches of glucose
176 metabolism (Figure 2A). Therefore, we first measured the steady-state levels of key glycolytic
177 and pentose phosphate pathway (PPP) intermediates, and trehalose in WT or *ubp3Δ* cells
178 using targeted LC-MS/MS. Glucose-6/fructose-6 phosphate (G6P/F6P) increased in *ubp3Δ*
179 cells (Figure 2C). Concurrently, trehalose, and the late PPP intermediates ribose 5-phosphate
180 (R5P) and sedoheptulose 7-phosphate (S7P) significantly increased in *ubp3Δ* cells (Figure 2C).

181 Since steady-state metabolite amounts cannot separate production from utilization,
182 in order to unambiguously assess if glycolytic flux is reduced in *ubp3Δ* cells, we utilized a pulse
183 labeling of $^{13}C_6$ glucose, following which the label incorporation into glycolytic and other
184 intermediates was measured. WT and *ubp3Δ* cells were grown in high glucose, pulsed with
185 $^{13}C_6$ glucose, and the relative ^{13}C label incorporation into glycolytic intermediates and
186 trehalose were measured, as shown in the schematic (Figure S2B). Note that because
187 glycolytic flux is very high in yeast, this experiment requires rapid pulsing and extraction of
188 metabolites in order to stay in a linear range to avoid label saturation. This experiment is
189 therefore more extensively described in extended supplementary methods and controls
190 shown in Figure S2C. We observed increased ^{13}C label incorporation into G6P/F6P as well as
191 trehalose in *ubp3Δ* cells (Figure 2D). The ^{13}C label incorporation into glycolytic intermediates
192 F1,6BP, G3P, 3PG and PEP were significantly decreased in *ubp3Δ* cells, suggesting decreased
193 glycolytic flux (Figure 2D). We next measured ethanol concentrations in WT and *ubp3Δ* cells,
194 and observed a significant decrease in ethanol concentration in *ubp3Δ* cells (Figure 2E). We
195 also measured the rate of ethanol formation in WT and *ubp3Δ* cells, by shifting these cells to
196 fresh, high glucose medium and measuring ethanol concentration over time. We observed a
197 decrease in rate of ethanol production in *ubp3Δ* cells, suggesting decreased fermentation rate
198 (Figure 2F).

199 Collectively, these results suggest that that reduced Pfk1 and GAPDH (in *ubp3Δ* cells)
200 decrease glucose flux via glycolysis and the resulting overflow diverts glucose flux away from
201 glycolysis, and towards trehalose biosynthesis and the PPP.

202

203 **Phosphate accumulates due to altered Pi homeostasis in *ubp3Δ* cells**

204 Since *ubp3Δ* cells had decreased glycolytic flux along with increased flux towards
205 trehalose synthesis, we next asked if such reallocations of glucose-derived metabolites could
206 explain the increased mitochondrial activity in *ubp3Δ* cells. Our hypothesis here was based on
207 the reasoning given below.

208 An existing idea that proposes a biochemical origin of the Crabtree effect is that there
209 may be internal competition for shared metabolites/co-factors between (cytosolic) glycolytic

210 and mitochondrial processes. Here, mitochondria cannot sufficiently access these
211 metabolites and are therefore repressed (Diaz-Ruiz et al., 2011; Koobs, 1972; Rodríguez-
212 Enríquez et al., 2001). Contextually, a plausible role for inorganic phosphate (Pi) in regulating
213 glucose-mediated mitochondrial repression can be conceived. Cytosolic glycolysis requires
214 rapid, high consumption of Pi (Mason et al., 1981; Rodríguez-Enríquez et al., 2001; Van
215 Heerden et al., 2014), and it is therefore possible that this might limit the Pi continuously
216 available for mitochondrial use (Brazy et al., 1982; Koobs, 1972), resulting in mitochondrial
217 repression. In this context, we and others had earlier hypothesized that the balance between
218 reactions that release vs consume Pi might explain global changes in Pi levels (Gupta &
219 Laxman, 2021). On the Pi consumption side, during glycolysis the GAPDH reaction converting
220 glyceraldehyde 3-phosphate (G3P) to 1,3 bisphosphoglycerate (1,3BPG) rapidly converts ADP
221 and Pi to ATP, resulting in a decrease in Pi levels and consequent increase in ATP, in the
222 presence of glucose (Hohmann et al., 1996; Van Heerden et al., 2014). The ATP formed from
223 glycolysis itself is a Pi donor for reactions such as nucleotide biosynthesis, polyphosphate
224 biosynthesis and protein phosphorylation (Gupta & Laxman, 2021; Hunter, 2012). When the
225 glycolytic flux is high, the consumption of Pi will be correspondingly high due to increased
226 ATP, nucleotide and polyphosphate synthesis (Austin & Mayer, 2020; Hohmann et al., 1996;
227 Ljungdahl & Daignan-Fornier, 2012). We therefore wondered if this reaction would limit
228 amounts of cytosolic Pi that remains available for the mitochondria, as hypothesized in an
229 illustration in Figure 3A. Notably, *ubp3Δ* cells have reduced GAPDH levels and decreased
230 glycolytic flux. Separately, reactions resulting in the release of Pi are often underappreciated
231 (Gupta & Laxman, 2021). In this regard, trehalose synthesis is a major Pi releasing reaction,
232 and a significant source of free Pi critical for Pi homeostasis (Gupta et al., 2019; Van Heerden
233 et al., 2014). Notably, flux through this reaction is also substantially higher in *ubp3Δ* cells.
234 Therefore, there appears to be both an increase in Pi release (via trehalose), coupled with
235 decreased Pi consumption, in *ubp3Δ* cells. We therefore asked if this series of events might
236 increase Pi in *ubp3Δ* cells (Figure 3A), and if so could this increased Pi availability lead to
237 increased mitochondrial activity (as hypothesized in Figure 4A)?

238 To test this, we first assessed Pi levels in *ubp3Δ* and WT cells. *ubp3Δ* cells had
239 significantly higher Pi compared to WT cells, and this increased Pi was comparable to Pi
240 amounts in WT cells grown in excess Pi medium (Figure 3B). Similarly, we compared Pi

241 amounts in the catalytically inactive Ubp3^{C469A} cells, where Pi amounts were increased (Figure
242 S3A). Therefore, the loss of Ubp3 increases intracellular Pi levels.

243 Next, we asked if *ubp3Δ* cells exhibit signatures of cells that are in a 'high Pi' state. *S.*
244 *cerevisiae* maintain internal Pi balance by concurrently controlling the expression of a set of
245 genes encoding Pi transporters and enzymes that can increase intracellular Pi, collectively
246 known as the Pho regulon (Mouillon & Persson, 2006; Secco et al., 2012). The Pho regulon is
247 induced under Pi limitation, and repressed when Pi is abundant (Gupta et al., 2019; Mouillon
248 & Persson, 2006). We assessed two major Pho proteins (Pho84: a high-affinity membrane Pi
249 transporter, and Pho12: an acid phosphatase) in WT and *ubp3Δ* cells in high glucose. WT cells
250 grown in high Pi were used as a control. *ubp3Δ* cells have lower amounts of Pho84 and Pho12
251 (Figure 3C). Further, when cells are shifted to low Pi for one hour, Pho84 and Pho12 increased
252 in *ubp3Δ* cells. This two observations are consistent with the interpretation that reduced
253 Pho84 and Pho12 amounts in *ubp3Δ* cells are because of increased Pi levels, and not due to
254 Ubp3 altering Pho regulon function itself (Figure 3C). These data also clarify earlier
255 observations from *ubp3Δ* cells which noted reduced Pho proteins (Isasa et al., 2015).
256 Therefore, *ubp3Δ* cells constitutively have higher Pi, and likely a consequent decrease in Pho
257 proteins.

258 We next asked if the increased Pi in *ubp3Δ* cells is because of altered G6P allocations
259 towards different end-points. In particular, the Pi release from trehalose synthesis
260 (conversion of trehalose 6-phosphate to trehalose) can be a major source of cytosolic Pi
261 (Gupta et al., 2019; Gupta & Laxman, 2021). We therefore assessed the contribution of
262 increased trehalose synthesis towards the high Pi levels observed in *ubp3Δ* cells, by estimating
263 Pi levels in WT and *ubp3Δ* cells in the absence of trehalose 6-phosphate phosphatase (Tps2),
264 which catalyzes the Pi releasing step in trehalose synthesis. Notably, loss of Tps2 in *ubp3Δ*
265 cells resulted in a significant decrease in Pi (Figure 3D). There was no further difference in Pi
266 between *tps2Δ* and *ubp3Δtps2Δ* cells (Figure 3D). As an added control, we assessed trehalose
267 in WT and *ubp3Δ* cells in the absence of Tps2, and found no difference (Figure S3B). These
268 data show that increasing G6P flux towards trehalose biosynthesis is a major source of the
269 increased Pi in *ubp3Δ* cells.

270 Since the major GAPDH isozymes, Tdh2 and Tdh3, are reduced in *ubp3Δ* cells, we
271 asked if a reduction in GAPDH can also decrease Pi consumption and increase Pi. To assess
272 this, we generated a strain where Tdh2 and Tdh3 are deleted. *tdh2Δtdh3Δ* cells exhibit a
273 growth defect, but are viable, permitting further analysis. *tdh2Δtdh3Δ* cells had higher Pi
274 levels in high glucose (Figure 3E). Expectedly, we also observed a decrease in free ethanol in
275 *tdh2Δtdh3Δ* cells (Figure S3C), along with an accumulation of glycolytic intermediates F1,6 BP
276 and G3P, and decreased 3PG and PEP (Figure S3D). However, G6P and trehalose levels
277 between WT and *tdh2Δtdh3Δ* cells were comparable (Figure S3D, S3E). These data sugest that
278 unlike *ubp3Δ* cells, the increased Pi in *tdh2Δtdh3Δ* cells primarily comes only from decreased
279 Pi consumption (GAPDH step), and not from a combination of increased Pi synthesis (from
280 increased trehalose synthesis) as well as decreased Pi consumption (due to decreased
281 GAPDH). To further confirm that the increase in Pi in *ubp3Δ* and *tdh2Δtdh3Δ* cells in high
282 glucose is because of altered glucose flux, we measured the Pi in these cells growing in a
283 gluconeogenic medium – 2%, ethanol. In this scenario, the GAPDH catalyzed reaction is
284 reversed, converting 1,3BPG to G3P, and this would release and not consume Pi. Compared
285 to WT cells, the Pi levels decreased in *ubp3Δ* and *tdh2Δtdh3Δ* cells (Figure S3F), suggesting
286 that the changes in Pi in these mutants is driven by change in the balance of Pi release or
287 consumption.

288 These results indicate that the combined effect of increased Pi release coming from
289 trehalose synthesis, and decreased Pi consumption from reduced GAPDH collectively increase
290 the Pi levels in *ubp3Δ* cells. We therefore wondered, could the availability of Pi in the
291 cytoplasm, based on these arms of glucose metabolism determine mitochondrial repression?

292

293 **Phosphate availability dictates mitochondrial activity**

294 In other words, could there be Pi budgeting between cytosolic glycolysis and
295 mitochondria, to regulate Pi availability within the mitochondria, and therefore mitochondrial
296 activity (Figure 4A)? To test this, we first asked if the mitochondria in *ubp3Δ* cells have
297 increased Pi. Mitochondria were isolated by immunoprecipitation from WT and *ubp3Δ* cells,
298 the efficiency of mitochondria isolation was analyzed (Figure S4A) and relative Pi levels

299 compared. Pi levels were normalised to the protein levels of the mitochondrial matrix protein
300 Idh1 (isocitrate dehydrogenase) in isolated mitochondria, since Idh1 protein levels did not
301 decrease in *ubp3Δ* cells (Figure S4B), and also consistent with (Isasa et al., 2015). We observed
302 significantly higher mitochondrial Pi in *ubp3Δ* cells (Figure 4B). We next asked if the increased
303 mitochondrial activity in *ubp3Δ* cells is a consequence of high Pi. If this were the case, the
304 *tdh2Δtdh3Δ* cells should partially phenocopy *ubp3Δ* cells with respect to mitochondrial
305 activity. We first assessed mitochondrial membrane potential in *tdh2Δtdh3Δ* cells.
306 *tdh2Δtdh3Δ* cells have higher mitotracker intensity compared to WT cells (Figure S4C). Next,
307 we measured Cox2 protein, and observed that Cox2 levels are significantly higher in
308 *tdh2Δtdh3Δ* cells (Figure 4C). Finally, we measured basal OCR in *tdh2Δtdh3Δ* cells. Consistent
309 with the mitotracker and Cox2 results, a high basal OCR in *tdh2Δtdh3Δ* cells was also observed
310 (Figure 4D). Therefore, *tdh2Δtdh3Δ* cells have high mitochondrial activity, comparable to
311 *ubp3Δ* cells.

312 We next asked if increased Pi is necessary to increase mitochondrial activity in both
313 *ubp3Δ* and *tdh2Δtdh3Δ* cells. While glycolysis is defective in *ubp3Δ* and *tdh2Δtdh3Δ* cells,
314 there are key differences in the nodes of regulation in these respective cells. Therefore, it is
315 necessary to distinguish the effect of high Pi vs. only the effect of low glycolysis in activating
316 mitochondria in these mutants. Since *ubp3Δ* cells have an ~30% increase in Pi levels, we asked
317 what would happen to mitochondrial activity if we brought down the levels of Pi in *ubp3Δ*
318 cells to that of WT cells. Logically, if only decreased glycolysis (independent of Pi) is sufficient
319 to activate mitochondria, merely bringing down the Pi levels in *ubp3Δ* cells (while maintaining
320 the low glycolysis in *ubp3Δ* cells) should not affect mitochondrial activity. Notably, *ubp3Δ* cells
321 grown in low (1 mM) Pi have Pi levels similar to WT cells in standard (normal Pi) medium
322 (Figure S4D). *ubp3Δ* cells grown in low Pi also had decreased ethanol, suggesting reduced
323 glycolysis (Figure S4E). Therefore, we used this condition to further understand the role of Pi
324 in inducing mitochondrial function. We first measured the mitochondrial membrane potential
325 in *ubp3Δ* cells and *tdh2Δtdh3Δ* cells. Mitotracker fluorescence decreased in both *ubp3Δ* cells
326 and *tdh2Δtdh3Δ* cells in low Pi (Figure S4F). This suggests that increased Pi in *ubp3Δ* and
327 *tdh2Δtdh3Δ* cells is required for increasing mitochondrial membrane potential. Note: basal
328 mitotracker fluorescence in WT cells also decreases in low Pi, consistent with a necessary role
329 of Pi levels in regulating mitochondrial activity (Figure S4F). Next, we measured Cox2 protein

330 in *ubp3Δ* cells and *tdh2Δtdh3Δ* cells in low Pi. Cox2 levels were significantly reduced in both
331 *ubp3Δ* and *tdh2Δtdh3Δ* cells in this condition (Figure 4E). Finally, we measured OCRs in these
332 cells under the same conditions. Consistent with both reduced mitotracker intensity and Cox2
333 levels, basal OCR also decreased in both *ubp3Δ* and *tdh2Δtdh3Δ* cells in low Pi (Figure 4F).
334 These data collectively indicate that high intracellular Pi is necessary to increase
335 mitochondrial activity in *ubp3Δ* and *tdh2Δtdh3Δ* cells.

336 Next, we asked how mitochondrial Pi transport regulates mitochondrial activity. Mir1
337 and Pic2 are yeast mitochondrial Pi transporters, with Mir1 being the major Pi transporter
338 (Murakami et al., 1990; Zara et al., 1996). We first limited mitochondrial Pi availability in
339 *ubp3Δ* cells by knocking-out only *MIR1*. In *mir1Δ* cells, the increase in Cox2 observed in *ubp3Δ*
340 cells was no longer observed (Figure 4G). Consistent with this, we observed no increase in the
341 basal OCR in *mir1Δubp3Δ* cells compared to *mir1Δ* cells (Figure 4H). This indicates that
342 mitochondrial Pi transport is necessary for increasing mitochondrial activity in *ubp3Δ* cells.
343 Furthermore, the loss of Mir1 resulted in a significant decrease in Cox2 protein as well as basal
344 OCR even in WT cells (Figure 4G, Figure 4H). These data suggest that mitochondrial Pi
345 transport (via Mir1) is critical for maintaining basal mitochondrial activity even in high glucose.

346 We also assessed what happens to mitochondrial Pi transporters Mir1 and Pic2 in
347 *ubp3Δ* cells, compared to WT cells. No significant increase in Mir1 and Pic2 could be observed
348 (Figure S4G). This data is consistent with the scenario where *ubp3Δ* cells increase
349 mitochondrial Pi primarily by increasing available Pi pools, and not by merely increasing the
350 Pi transporters.

351 Collectively, these data suggest the possibility that increased cytosolic Pi can increase
352 the mitochondrial Pi pool, which in turn increases mitochondrial activity. Decreasing
353 mitochondrial Pi by either reducing total Pi, or by selectively blocking mitochondrial Pi
354 transport decreases mitochondrial activity.

355 **Mitochondrial Pi availability controls glucose-mediated mitochondrial repression**

356 So far, our data suggest a direct role for the pool of Pi available for the mitochondria,
357 in regulating mitochondrial activity. Could this, therefore, be a general mechanism of
358 controlling glucose-mediated mitochondrial repression?

359 To test this, we first asked how important mitochondrial Pi transport was for the
360 switch to increased respiration. Highly fermentative yeast cells increase respiration in low
361 glucose (Broach, 2012; Gasmi et al., 2014). We measured the basal OCR in WT and *mir1Δ* cells
362 after switching from high (2%) to low (0.1%) glucose. WT cells showed a significant increase
363 in the basal OCR (Figure 5A) while *mir1Δ* cells did not show an increase in basal OCR (Figure
364 5A). An alternate scenario wherein cells increase mitochondrial activity is after glycolytic
365 inhibition. We asked what happens upon 2DG treatment, in the context of mitochondrial Pi
366 transport and mitochondrial activation. WT cells increased their basal OCR upon a 1-hour
367 treatment with 2DG, indicating increased respiration (Figure 5B). However, this increase was
368 not observed in *mir1Δ* cells upon 2DG treatment (Figure 5B). We next measured the
369 mitochondrial membrane potential with increasing concentrations of 2DG. Mitotracker
370 fluorescence increased with an increase in 2DG in WT cells. However, this was not observed
371 in *mir1Δ* cells (Figure S5A). These data indicate that mitochondrial Pi transport is necessary
372 for increasing mitochondrial activity under glucose derepression.

373 Next, we asked if the switch to higher respiration involves upregulating the
374 mitochondrial Pi transporter. We measured Mir1 protein in WT cells in a high (2%) glucose
375 and after shifting cells to low (0.1%) glucose. Mir1 increases significantly upon a shift to low
376 glucose, suggesting that Mir1 is glucose repressed (Figure 5C). High Mir1 was also observed
377 in cells grown in 2% ethanol (where glucose is absent), compared to that of glucose-grown
378 cells (Figure S5B), further reiterating that Mir1 is glucose-repressed. These data collectively
379 suggest that decreased Pi (due to high Pi consumption in glycolysis), coupled with decreased
380 Mir1 protein levels, results in reduced mitochondrial Pi under high glucose.

381 So far, these results indicate that mitochondrial Pi transport is required for
382 mitochondrial activity, and that decreasing mitochondrial Pi availability represses
383 mitochondria. Therefore, we next asked whether increasing mitochondrial Pi is sufficient to
384 increase mitochondrial activity in high glucose. Since WT cells in high Pi have higher Pi levels
385 (Figure 3B), it could be prematurely assumed that directly adding Pi to cells grown in high
386 glucose might increase the Pi accessible to mitochondria, and thereby mitochondrial
387 respiration. Alternately, since glycolytic flux is maximal in high glucose, merely supplementing
388 Pi to the cells might be insufficient to increase Pi access to the mitochondria, but might only
389 further fuel glycolysis (as was originally obseved by Harden and Young in 1908. Interestingly,

390 supplementing more Pi to the medium did not result in an increase in mitochondrial Pi.
391 Furthermore, WT cells grown in a high Pi medium have further decreased levels of
392 mitochondrial Pi (Figure S5C). Consistent with this, directly adding Pi to cells grown in high
393 glucose have decreased basal OCR (Figure S5D). This suggests that in high glucose, further
394 supplementing Pi might only serve to sustain glycolysis, but not allow increased Pi access to
395 the mitochondria.

396 To further dissect this possibility, we treated cells with glycolytic inhibitor 2DG to
397 inhibit glycolysis, and then subsequently added Pi and measured the OCR (Figure S5E). In this
398 case, we observed a significant increase in basal OCR upon supplementing Pi (Figure S5E).
399 Collectively this suggests that decreasing glycolysis, and increasing Pi levels can now increase
400 respiration. Next, to unambiguously test the extent of mitochondrial activation based on Pi
401 availability, we isolated mitochondria, and estimated activity *in vitro* with increasing Pi.
402 Isolated mitochondria were incubated with 1 mM pyruvate, 1 mM malate, 0.5 mM ADP and
403 increasing Pi (KH_2PO_4) concentrations, and mitochondrial activity was estimated.
404 Mitochondrial activity increased with increased Pi, with maximum activity observed with 25
405 mM Pi (Figure 5D). This reconstitution reveals the extent of mitochondrial activation based
406 purely on the availability of accessible external Pi. Next, in a complementary experiment, we
407 overexpressed Mir1 in wild-type cells (under a G6PD promoter), in order to forcibly increase
408 Pi within mitochondria. For this experiment, we selected clones with an ~2-fold increase in
409 Mir1 protein (Figure S5F). We first measured Cox2 protein in the Mir1 overexpressing (Mir1-
410 OE) cells and observed an increase in Cox2 (Figure 5E). Next, we measured the basal OCR in
411 Mir1-OE cells and observed a significant increase in basal OCR (Figure 5F). Therefore,
412 increasing mitochondrial Pi transport alone is sufficient to increase mitochondrial activity in
413 high glucose.

414 The transport of pyruvate into the mitochondria is required for mitochondrial
415 respiration (McCommis & Finck, 2015). We asked where Pi availability stands in a hierarchy
416 of necessary constraints with respect to mitochondrial pyruvate transport, as a requirement
417 for mitochondrial derepression. We measured the amounts of the Mpc3 subunit (critical for
418 mitochondrial respiration) of the mitochondrial pyruvate carrier (MPC) complex (Bender et
419 al., 2015; Timoń-Gómez et al., 2013). Mpc3 protein increases in *ubp3Δ* cells (Figure S5G),
420 correlating with the increased mitochondrial activity. Interestingly, when *ubp3Δ* cells are

421 grown in low Pi, Mpc3 protein further increased (Figure S5G), but as shown earlier this
422 condition cannot increase OCR or mitochondrial activity (Figure 4F, S4F). Next, we measured
423 the levels of Mpc3 in WT and *mir1Δ* cells in 2% glucose and upon shifting to low (0.1%)
424 glucose. The basal levels of Mpc3 decrease in *mir1Δ* cells, but upon shifting to low glucose,
425 Mpc3 levels increase in both WT and *mir1Δ* cells, with comparatively higher levels in *mir1Δ*
426 cells (Figure S5H). These data now allow a precise interpretation. Even under conditions
427 where Mpc3 levels are high (*ubp3Δ* cells in low Pi medium, and *mir1Δ* cells in low glucose),
428 mitochondrial activity remains low if Pi is restricted (Figure 4F, 4H). This indicates that even
429 though changes in Mpc3 levels accompanies the change in mitochondrial activity,
430 mitochondrial Pi availability is the primary driver of mitochondrial activity and respiration,
431 superseding Mpc3 protein. To test if Mpc3 is required for the increase in basal OCR upon
432 shifting from high to low glucose, we measured the basal OCR in WT and *mpc3Δ* cells. There
433 was no decrease in basal OCR in *mpc3Δ* cells in high glucose, and the basal OCR increased to
434 the same level as that of WT cells after shifting to 0.1% glucose (Figure S5I). These data,
435 suggest that Mpc3 is not required for the increase in basal OCR upon shifting to low glucose.
436 Finally, since Mpc3 changes with mitochondrial Pi availability (Figure S5G, S5H), we measured
437 Mpc3 in the Mir1OE strain. No further changes in Mpc3 were observed in Mir1OE cells (Figure
438 S5J), indicaging that increasing mitochondrial Pi alone need not increase Mpc3 levels. The
439 increase in Mpc3 levels instead best correlates with decreased glycolysis (*ubp3Δ* cells-Figure
440 S5G, *ubp3Δ* cells in low Pi-Figure S5G, low glucose medium-Figure S5H), suggesting that Mpc3
441 protein is repressed during glycolysis. Overall, even though Mpc3 levels respond to changes
442 in glycolytic rate, increased Mpc3 is insufficient to increase mitochondrial activity and
443 respiration in the absence of adequate mitochondrial Pi. Contrastingly, increasing
444 mitochondrial Pi is necessary and sufficient to drive increased mitochondrial activity and
445 respiration.

446 Finally, we asked how dependent growth under 2DG treatment is towards
447 mitochondrial Pi transport. In the presence of 2DG, WT cells exhibit a small decrease in
448 growth. In contrast, *mir1Δ* cells exhibit a severe growth defect upon 2DG treatment, unlike
449 WT cells (Figure 5G), revealing a synergetic effect of combining 2DG with inhibiting
450 mitochondrial Pi transport. This, along with data shown in Figure 5B, show that mitochondrial
451 Pi transport is required for cells to switch to more respiration upon glycolytic inhibition, and

452 limiting mitochondrial Pi makes cells hypersensitive to 2DG. Therefore, the combined
453 inhibition of glycolysis and mitochondrial Pi transport can effectively restrict the growth of
454 highly glycolytic cells.

455 Collectively, we find that mitochondrial Pi availability controls glucose-mediated
456 mitochondrial repression. Increasing available pools of Pi to enter the mitochondria is
457 sufficient to induce mitochondrial activity regardless of glucose availability.

458

459 **Discussion**

460 In this study, we highlight a central role for Pi allocations between cytosolic glycolysis
461 and mitochondrial processes - both of which compete for Pi - as a driver of glucose-mediated
462 mitochondrial repression. This concept is schematically illustrated in Figure 5H. Ubp3 can
463 control this process (Figure 1), by allowing high glycolytic flux by maintaining the amounts of
464 the glycolytic enzymes phosphofructokinase (Pfk1) and GAPDH (Tdh2 and Tdh3). At high rate
465 of fermentation and growth in *S. cerevisiae*, glycolytic enzymes levels are optimal for
466 maintaining the high glycolytic rate, and therefore, change in the enzyme levels will have a
467 direct, proportionate effect on flux (Grigaitis & Teusink, 2022). The loss of Ubp3 results in
468 decreased glycolytic flux, due to a decrease in these key enzymes, collectively resulting in a
469 systems-level, mass-action based rewiring of glucose metabolism where more G6P is routed
470 towards trehalose synthesis and the PPP (Figure 2, Figure 5H). Indeed, previous studies also
471 find that inhibiting phosphofructokinase reroutes glucose flux from glycolysis to PPP
472 (Hollinshead et al., 2016; Miyazawa et al., 2017; Yi et al., 2012), and our study may permit
473 additional, contextualized interpretations of these results. Such reallocations of glucose flux
474 collectively result in an overall Pi increase, coming from the combined effect of increased Pi
475 release (from trehalose synthesis), and decreased Pi consumption (via reduced GAPDH). This
476 changes the intracellular Pi economy to increase the Pi pool available to mitochondria, and
477 thereby increases mitochondrial activity (Figure 4, Figure 5H). Notably, increased
478 mitochondrial Pi is necessary and sufficient to increase respiration in high glucose (Figure 4,
479 Figure 5). Mitochondrial Pi transport is necessary to maintain mitochondrial activity in high
480 glucose, and also to increase mitochondrial activity in low glucose (Figure 4, Figure 5). Finally,

481 the mitochondrial Pi transporter Mir1 itself decreases in high glucose (Figure 5). Therefore,
482 along with high Pi consumption, this glucose-dependent repression of Mir1 restricts
483 mitochondrial Pi availability (and thereby activity) in high glucose. These data reveal a central
484 role for Pi budgeting in regulating mitochondrial activity, and mediating mitochondrial
485 repression.

486 Traditionally, loss-of-function mutants of metabolic enzymes are used to understand
487 metabolic state regulation. This approach makes nuanced investigations impossible, since
488 metabolic enzymes are often essential for viability. Furthermore, metabolic pathways have
489 multiple, contextually regulated nodes, through which cells maintain their metabolic state.
490 Therefore, alternate approaches to identify global regulators of metabolic states (as opposed
491 to single enzymes), might uncover ways via which multiple nodes are simultaneously tuned,
492 and reveal unanticipated systems-level principles of metabolic state rewiring. Such regulators
493 can include kinases/phosphatases, ubiquitin ligases/ deubiquitinases,
494 acetyltransferases/deacetylases, etc., all of which can dynamically regulate multiple nodes. In
495 this context, the proteostatic regulation of metabolism by reversible ubiquitination (and the
496 roles of DUBs therein) remain underexplored, perhaps because of the challenges of
497 identifying specific substrates. In this study of glucose-mediated mitochondrial repression,
498 the loss of the DUB Ubp3 decreases glycolytic flux by reducing the enzymes at two critical
499 nodes in the pathway - Pfk1 and GAPDH. A consequence of both these steps is that while they
500 are coupled to Pi consumption, unlike complete loss of function mutants, a reduction in
501 amounts will not kill cells but rewire metabolic flux. By 'hitting' multiple steps in glycolysis
502 simultaneously, *ubp3Δ* cells have decreased Pi consumption, as well as increased Pi release.
503 Such a cumulative phenomenon reveals more than, for example, inhibiting only GAPDH alone,
504 where the increase in Pi is only due to reduced Pi consumption, and not from increased
505 trehalose biosynthesis. Similarly, 2DG shuts down a majority of glycolysis (instead of
506 dampening the PFK and GAPDH steps), and this results in an acute metabolic rewiring. Our
507 serendipitous identification of a general regulator, which regulates multiple steps to change
508 the metabolic environment, suggests a general basis of mitochondrial regulation that would
509 have otherwise remained hidden. Separately, finding the substrates of Ubp3 and how Ubp3
510 regulates glycolytic enzymes are exciting future research questions requiring concurrent
511 innovations in accessible chemical-biological approaches.

512 This study highlights the importance of intracellular Pi balance in maintaining
513 metabolic states. Because phosphates are required everywhere, it is challenging to identify
514 hierarchies of Pi-dependent processes in metabolic state regulation (Gupta & Laxman, 2021).
515 Phosphate transfer reactions are the foundation of metabolism, driving multiple,
516 thermodynamically unfavorable reactions (Kamerlin et al., 2013; Westheimer, 1987).
517 Contextually, the laws of mass action predicts that the relative rates of these reactions will
518 regulate overall Pi balance, and contrarily the allocation of Pi to these reactions will determine
519 the rate of these Pi-dependent reactions (Gupta & Laxman, 2021; Van Heerden et al., 2014).
520 One way by which cells might control Pi allocations for different reactions comes from
521 compartmentalizing Pi in organelles, to spatially restrict Pi availability (Booth & Guidotti,
522 1997; Solesio et al., 2021; Vila et al., 2022). Alongside this, the rates of reactions that release
523 and utilize Pi would also determine relative Pi allocations (Gupta & Laxman, 2021; Van
524 Heerden et al., 2014). Our data collectively suggest a paradigm where the combination of
525 these factors regulates mitochondrial activity. In high glucose, in cells with high glycolytic flux
526 (like yeast), mitochondrial Pi availability becomes restricted due to the greater utilization of
527 Pi in glycolysis compared to mitochondria. A consequent limitation in mitochondrial Pi could
528 thereby cause mitochondrial repression. Consistent with this idea, a rapid decrease in
529 intracellular Pi upon glucose addition has been observed (Koobs, 1972; Rodríguez-Enríquez et
530 al., 2001; Sussman et al., 1980). Further, supplementing Pi correlates with decreased
531 mitochondrial repression in tumors (Brin & McKee, 1956; Koobs, 1972; Wu & Racker, 1959).
532 Concurrently, the levels of the mitochondrial Pi transporter Mir1 is also glucose-repressed,
533 further limiting mitochondrial Pi uptake. By increasing Pi through a systems-level rewiring of
534 glucose metabolism (such as in *ubp3Δ* cells), cells collectively increase mitochondrial access
535 to Pi. Since Pi is critical for multiple mitochondrial processes, this relative Pi budgeting can
536 determine mitochondrial activity. Notably, even though directly supplementing Pi decreases
537 mitochondrial repression in tumors (Koobs, 1972), our data suggests that this alone might not
538 be sufficient in highly glycolytic cells such as yeast. In these conditions, adding Pi further
539 increases glycolysis, as was first observed during the beginnings of modern biochemistry
540 (Harden & Young, 1908). Indeed, directly supplementing Pi to glycolytic cells decreases
541 mitochondrial Pi and respiration (Figure S5). Interestingly, supplementing Pi under conditions
542 of low glycolysis (where mitochondrial Pi transport is already enhanced), as well as directly
543 supplementing Pi to isolated mitochondria, increases respiration (Figure 5, S5). Therefore, in

544 order to deprepress mitochondria, a combination of increasing Pi along with decreasing
545 glycolysis is required. An additional explanation for this phenomenon is the change in
546 intracellular pH that accompanies the changes in glycolytic state. The cytosolic pH in highly
547 glycolytic cells is ~7 and decreasing glycolysis results in cytosolic acidification (Dechant et al.,
548 2010; Orij et al., 2011). Since mitochondrial Pi transport is itself dependent on the proton
549 gradient, a low cytosolic pH would favour mitochondrial Pi transport (Hamel et al., 2004).
550 Therefore, under conditions of decreased glycolysis (2DG treatment, deletion of Ubp3, and
551 decreased GAPDH activity), where cytosolic pH is acidic, increasing cytosolic Pi might
552 indirectly increase mitochondria Pi transport, thereby leading to increased respiration.
553 Alternately, increasing mitochondrial Pi transporter amounts to enhance mitochondrial Pi
554 uptake can also achieve the same result, as seen by overexpressing Mir1 (Figure 5). A similar
555 observation has been reported in *Arabidopsis*, reiterating an evolutionarily conserved role for
556 mitochondrial Pi in controlling respiration (Jia et al., 2015). Relatedly, glycolytic inhibition can
557 suppress cell proliferation in Warburg-positive tumors (Pelicano et al., 2006), or inflammatory
558 responses (Soto-Heredero et al., 2020). The glucose analog 2-deoxyglucose (2DG) inhibits the
559 hexokinase and phosphoglucose isomerase catalyzed steps (Laussel & Léon, 2020), and has
560 been used to inhibit 'Warburg' positive cancer cells (Aft et al., 2002; O'Neill et al., 2019).
561 However, these cells survive by switching to mitochondrial respiration (Lu et al., 2015; Oliveira
562 et al., 2021; Shiratori et al., 2019), requiring alternate approaches to prevent their
563 proliferation (Cheng et al., 2012). Inhibiting mitochondrial Pi transport in combination with
564 glycolytic inhibition could effectively restrict the proliferation of Warburg/Crabtree positive
565 cells. As seen in *ubp3Δ* cells, this mode of regulating Pi balance will therefore have systems-
566 level changes in the metabolic milieu, enhancing certain types of metabolic reactions to
567 thereby control metabolic states.

568 Since its discovery in the 1920s, the phenomenon of accelerated glycolysis with
569 concurrent repression of mitochondrial activity has been intensely researched. Yet, a
570 parsimonious explanation of the biochemical basis of glucose-mediated mitochondrial
571 repression remains missing. One hypothesis suggests that the availability of glycolytic
572 intermediates might determine a biochemical basis of the Crabtree effect. F1,6BP inhibits
573 complex III and IV of the electron transport chain (ETC) in Crabtree positive yeast (Diaz-Ruiz
574 et al., 2011; Díaz-Ruiz et al., 2008; Hammad et al., 2016; Lemus et al., 2018). Similarly, the

575 ratio between G6P and F1,6BP regulates the extent of mitochondrial repression (Díaz-Ruiz et
576 al., 2008; Lemus et al., 2018). Therefore, glycolytic intermediates might trigger the Crabtree
577 effect (Hammad et al., 2016). Our study now clarifies these hypotheses, placing Pi centre
578 stage. Although G6P/F6P accumulates in *ubp3Δ* cells (Figure 2C), this is not the case in
579 *tdh2Δtdh3Δ* (GAPDH mutant) cells (Figure S3D), suggesting that G6P/F6P accumulation in
580 itself is not the prime criterion to increase mitochondrial activity. Separately, the competition
581 for common metabolites/co-factors between glycolysis and respiration (such as ADP, Pi or
582 pyruvate) could drive this phenomenon (Diaz-Ruiz et al., 2011; Koobs, 1972). In *ubp3Δ* cells
583 growing in low Pi, there is decreased glycolysis (Figure S4E) concurrent with increased
584 mitochondrial pyruvate transporter (Mpc3) levels (Figure S5G). According to the above
585 hypothesis, this should increase mitochondrial activity. However, these cells have decreased
586 mitochondrial activity. Similarly, switching to low glucose increases Mpc3 levels in *mir1Δ* cells,
587 but cannot increase mitochondrial respiration (Figure S5H, 5A), and basal OCR in *mpc3Δ* cells
588 increases in low glucose similar to WT cells (Figure S5I). Therefore, in alternate scenarios, such
589 as contexts where amino acids can fuel TCA cycle, Mpc3 is not critical to switch to high
590 respiration. These collectively reiterate a dominant role of mitochondrial Pi transport (and Pi
591 access) in regulating mitochondrial respiration. Our data also clarifies or contextualizes
592 observations from other model systems where mitochondrial Pi transport seems to regulate
593 mitochondrial respiration (Poncet et al., 2006; Scheibye-Knudsen & Quistorff, 2009; Seifert et
594 al., 2015).

595 Relying on parsimony, we propose that Pi access to the mitochondria provides a
596 simple explanation for the biochemical basis of the Crabtree effect. A single-step event in
597 evolution, of either reducing mitochondrial Pi transporter amounts, and/or increasing
598 glycolytic flux (to deplete cytosolic Pi), will result in whole-scale metabolic rewiring to repress
599 mitochondria. Such an event need not invoke the evolution of elaborate regulatory
600 mechanisms where glycolytic intermediates allosterically inhibit mitochondrial processes,
601 and such regulatory events can easily be imagined as subsequent adaptations to enforce
602 mitochondrial repression. Given the central role played by Pi in cells, it is not surprising that
603 something as fundamental as access to Pi could determine mitochondrial activity. The basis
604 of the Crabtree effect can be explained by this simple competition for Pi between glycolysis
605 and mitochondrial processes. The rapid incorporation of Pi into faster glycolysis gives cells a

606 proliferation advantage, while also sequestering Pi in the form of usable ATP. Over the course
607 of evolution, this can drive other regulatory mechanisms to enforce mitochondrial repression,
608 plausibly leading to the currently observed complex regulatory networks and signaling
609 programs and the Crabtree effect we know today.

610

611 ## Materials and methods

612 ### Yeast strains, media, and growth conditions

613 A prototrophic CEN.PK strain of *Saccharomyces cerevisiae* (WT) (J.P. van Dijken et al., 2000)
614 was used. Strains used in this study are listed in Table S1. Gene deletions and chromosomal C
615 terminal tagged strains were generated by standard PCR mediated gene deletion or tagging,
616 using drug resistance markers (Longtine et al., 1998). Cells were grown overnight in a standard
617 high glucose, at 30°C, and subcultured in the required medium. For experiments involving a
618 shift to a no-Pi or low glucose medium, cells were subcultured in high glucose till OD_{600}~0.6,
619 pelleted by centrifugation (1000 x g, 2 min at RT), washed, and shifted to no-Pi or low glucose
620 medium for 1 hour. The detailed media compositions and growth conditions are described in
621 extended methods (supplement file 1).

622 ### Mitotracker fluorescence assay

623 Cells were grown to OD_{600}~0.6, 1 OD_{600} cells were collected by centrifugation (1000 x g, 1 min
624 at RT), and resuspended in 1 ml fresh media. Mitotracker CMXRos (M7512 ThermoFisher) was
625 added to a final concentration of 200 nM and incubated at 30°C in a shaking incubator. Cells
626 were washed and resuspended in fresh media and fixed with 2% formaldehyde for 20
627 minutes. Fixed cells were washed in 1xPBS, pH 7.4, and resuspended in 1 ml 1xPBS. 300 µl of
628 this was aliquoted onto 96 well plates in replicates. Mitotracker fluorescence was measured
629 using Thermo Varioscan™ LUX multimode plate reader at 579/599 excitation/emission
630 wavelengths. Mitotracker fluorescence readings were normalized using OD_{600} of each sample
631 and the relative fluorescence intensity was calculated. Statistical significance was calculated
632 using unpaired Student's t-test (GraphPad prism 9.0.1).

633 ### Mitotracker based screen to identify DUBs that regulate mitochondrial repression

634 The deubiquitinase deletions were made by PCR mediated gene deletion, DUB deletion
635 mutants generated were grown in high glucose and the mitochondrial membrane potential
636 measured by the mitotracker assay described earlier. For performing the screen, the 19 DUB
637 knockouts were divided into two groups- each containing 10 and 9 DUB KOs respectively and
638 the screen was performed separately for each group in replicates. WT cells grown in high
639 glucose indicated the basal mitochondrial potential and WT cells grown in ethanol was used
640 as a positive control for each group. The mitotracker fluorescence intensity were normalised
641 to OD_{600} of each mutant and the fluorescence intensity relative to the WT cells were calculated.
642 The relative fluorescence intensity for the replicate samples are shown in supplementary
643 figure S1A, mean fluorescence intensities of the replicates (relative to WT) were calculated
644 and plotted as heat maps (Figure 1C).

645 **CRISPR-Cas9 based mutagenesis**

646 To generate the $Ubp3^{C469A}$ strain, cells were transformed a constitutive Cas9 expressing
647 plasmid (Addgene plasmid 43802, (Dicarlo et al., 2013)). Guide RNA (gRNA) sequences
648 (forward and reverse) were annealed and cloned into a pMEL13 plasmid. Strains were then
649 transformed with gRNA plasmid and homology repair (HR) fragments with the base pair
650 mutation. The HR fragment was generated by site-directed mutagenesis PCR. Positive clones
651 were selected using drug, and sequenced to confirm the mutation. Oligonucleotides used are
652 listed in Table S2.

653 **Serial dilution growth assay**

654 For serial dilution-based growth assays, cells were grown in standard high glucose to
655 OD_{600}~0.8, collected by centrifugation (1000 x g, 1 min at RT), washed with water, serial
656 dilutions made (OD_{600}=1, 0.1, 0.01, 0.001, 0.0001), 5 µl of each dilution were spotted onto agar
657 plates, incubated at 30°C and growth monitored.

658 **Protein extraction and Western blotting**

659 The cells were grown in the indicated medium to OD_{600}~0.8 and pelleted by centrifugation
660 (1000 x g, 2 min at RT). Total protein was precipitated and extracted using trichloroacetic acid
661 (TCA), and resuspended in SDS/glycerol buffer as described earlier (Vengayil et al., 2019). For

662 loading controls, the same gel fragments were stained using Coomassie R-250. All western
663 blot quantifications were done using ImageJ software. Graphs were plotted using GraphPad
664 prism 9.0.1. Detailed protocol is described in extended methods (supplement file 1).

665 **Basal OCR measurement using Seahorse assay**

666 The basal OCR was measured using Agilent Seahorse XFe24 analyzer. 1 ml of the XF Calibrant
667 solution was aliquoted into each well of the utility plate and the sensor cartridge plate was
668 hydrated overnight as per the manufacturer's instructions. The sensor cartridge was loaded
669 with complex IV inhibitor sodium azide and equilibrated in the Seahorse XFe24 analyzer one
670 hour prior to the start of the assay. The culture plate was coated with 50 µl poly-L-lysine and
671 incubated for 1 hour at RT. Excess poly-L-lysine was removed and the plate dried at 30°C for
672 30 minutes. The cells were grown in standard high glucose to an OD_{600}~0.6. The samples were
673 aliquoted to poly-L-lysine coated wells at a final cell number in each well of ~3x10^5. The
674 plate was centrifuged for 2 min at 100xg (acceleration 2, brake 2) and incubated at 30°C for
675 30 minutes. The plate was loaded to the Seahorse XFe24 analyzer and basal OCR measured
676 over time. A minimum of three measurements were taken with intermittent 2 min mixing and
677 waiting steps. This was followed by sodium azide injection to the sample wells, and three
678 measurements were taken with intermittent 2 min mixing and waiting steps. The basal OCR
679 readings were normalized to the OD_{600} of samples in each well (for cell numbers), and graphs
680 were plotted using GraphPad prism 9.0.1.

681 **ATP assay**

682 The ATP levels were measured by ATP estimation kit (Thermo Fisher A22066). Detailed sample
683 collection protocol is described in extended methods (supplement file 1). The reaction
684 mixture was prepared as per manufacturer's instructions and 10 µl of sample was mixed with
685 90 µl of reaction mix and luminescence was measured using Sirius luminometer (Tiertek
686 Berthold). The ATP standards prepared in 20 mM Tris-HCl, pH 7.0 was used to plot the
687 standard curve and to estimate the ATP concentration in the samples. The relative ATP
688 concentrations were calculated, graphs were plotted and using GraphPad prism 9.0.1.

689 **Metabolite extraction and analysis by LC-MS/MS**

690 The steady state levels as well as relative ^{13}C label incorporation into metabolites were
691 estimated by quantitative LC-MS/MS methods as described in (Walvekar et al., 2018). The
692 detailed methodology is described in extended methods (Supplement file 1). All the peak
693 area measurements for the steady state and ^{13}C glucose flux experiments are listed in
694 supplement file 2.

695 **Ethanol estimation assay**

696 The ethanol concentration in the medium was estimated using potassium dichromate based
697 assay as described in (Sriariyanun et al., 2019) with modifications. The detailed protocol is
698 described in extended methods (Supplement file 1). The statistical significance was calculated
699 using unpaired Student's t-test (GraphPad prism 9.0.1).

700 **Malachite green based Pi estimation**

701 The cells were grown to OD_{600}~0.8, pelleted by centrifugation (1000 x g, 2 min at RT), pelleted
702 cells were washed and resuspended in 1 ml ice-cold HPLC grade water (to avoid Pi
703 contamination) and lysed by bead beating (3 x 20s, 1 min intermittent cooling). Lysates were
704 centrifuged (14000 rpm, 1 min at 4°C) and 800 µl of the clear supernatant collected. Protein
705 concentrations of the supernatant were estimated using BCA assay (BCA assay kit, G-
706 Biosciences). Lysates corresponding to 1µg total protein was used for the Pi estimation assay.
707 Pi estimation was done using a malachite green phosphate assay kit (Cayman chemicals,
708 10009325) as per the manufacturer's instructions. Statistical significance was calculated using
709 unpaired Student's t-test (GraphPad prism 9.0.1).

710 **Mitochondrial isolation by immunoprecipitation**

711 Mitochondria was isolated by immunoprecipitation as described in (Chen et al., 2017; Liao et
712 al., 2018) with modifications. The detailed sample preparation protocol is described in
713 extended methods (supplement file 1). The eluted mitochondria were used in malachite
714 green assay for Pi estimation or boiled with SDS-glycerol buffer for western blots.

715 For mitotracker assays with isolated mitochondria (Figure 5D), the mitochondria enriched
716 fraction resuspended in SEH buffer was centrifuged twice- 700 x g for 5mins and 1500 x g for
717 5 mins at 4°C. The supernatant was collected and centrifuged at 12000 x g for 10 mins at 4°C

718 and the pellet was resuspended in ice-cold SEH buffer. The protein concentration of this crude
719 mitochondria was estimated by BCA protein estimation assay and mitochondria
720 corresponding to 5 µg protein was incubated in 200 µl SEH buffer containing 1 mM pyruvate,
721 1 mM malate, 0.5 mM ADP and 0 – 50 mM KH_2PO_4 for 30 minutes at 30°C. Mitotracker
722 CMXROS was added at a final concentration of 200 nM, followed by incubation at 30°C for 30
723 minutes. The fluorescence intensities were measured using Thermo Varioscan™ LUX
724 multimode plate reader at 579/599 excitation/emission, and fluorescence intensities relative
725 to samples containing 0 mM KH2PO4 was calculated. Statistical significance was calculated
726 using unpaired Student's t-test (GraphPad prism 9.0.1).

727

728 **Acknowledgements**

729 We thank all SL lab members, Benjamin Tu, Anand Bachhawat and Vijay Jayaraman for critical
730 comments and suggestions on this manuscript. We acknowledge the use of
731 NCBS/inStem/CCAMP mass spectrometry facility for the use of LC-MS/MS instruments. We
732 thank Aayushee Khanna for help with experiments. V.V acknowledges the funding support
733 from DST-INSPIRE fellowship (IF170236), S.N and SA acknowledges the funding from
734 inStem/DBT PhD fellowship, S.V acknowledges the support from DBT-Wellcome Trust India
735 Alliance Early Career Fellowship (IA/E/16/1/502996), S.L acknowledges support from the
736 Department of Science and Technology (DST), Govt. of India SERB CRG grant
737 CRG/2019/004772, and institutional support from inStem.

738

739 **Author contributions**

740 VV and SL conceptualized the study and designed experiments. VV, SN, SA, SV performed
741 experiments. All data were analyzed by VV and SL, and specific experiments were analyzed by
742 SN, SA and SV. VV and SL wrote the manuscript, including inputs from SN, SA and SV. SL
743 secured funding for this study.

744

745 **References**

746 Abdel-Haleem, A. M., Lewis, N. E., Jamshidi, N., Mineta, K., Gao, X., & Gojobori, T. (2017).
747 The emerging facets of non-cancerous Warburg effect. *Frontiers in Endocrinology*,
748 *8*(OCT), 1–7. https://doi.org/10.3389/fendo.2017.00279
749 Aft, R. L., Zhang, F. W., & Gius, D. (2002). Evaluation of 2-deoxy-D-glucose as a
750 chemotherapeutic agent: Mechanism of cell death. *British Journal of Cancer*, *87*(7),
751 805–812. https://doi.org/10.1038/sj.bjc.6600547
752 Austin, S., & Mayer, A. (2020). Phosphate Homeostasis − A Vital Metabolic Equilibrium
753 Maintained Through the INPHORS Signaling Pathway. *Frontiers in Microbiology*, *11*,
754 1367. https://doi.org/10.3389/FMICB.2020.01367/BIBTEX
755 Bender, T., Pena, G., & Martinou, J.-C. (2015). Regulation of mitochondrial pyruvate uptake
756 by alternative pyruvate carrier complexes. *The EMBO Journal*, *34*(7), 911–924.
757 https://doi.org/10.15252/EMBJ.201490197
758 Booth, J. W., & Guidotti, G. (1997). Phosphate Transport in Yeast Vacuoles *. *Journal of*
759 *Biological Chemistry*, *272*(33), 20408–20413.
760 https://doi.org/10.1074/JBC.272.33.20408
761 Bouchez, C. L., Hammad, N., Cuvellier, S., Ransac, S., Rigoulet, M., & Devin, A. (2020). The
762 Warburg Effect in Yeast: Repression of Mitochondrial Metabolism Is Not a Prerequisite
763 to Promote Cell Proliferation. *Frontiers in Oncology*, *10*, 1333.
764 https://doi.org/10.3389/FONC.2020.01333/BIBTEX
765 Brazy, P. C., Mandel, L. J., Dennis, V. W., & Gullans, S. R. (1982). Metabolic Requirement for
766 Inorganic Phosphate by the Rabbit Proximal Tubule: EVIDENCE FOR A CRABTREE
767 EFFECT Metabolic Requirement for Inorganic Phosphate by the Rabbit Proximal Tubule
768 EVIDENCE FOR A CRABTREE EFFECT. *J Clin Invest*, *70*(1), 53.
769 https://doi.org/10.1172/JCI110603
770 Brin, M., & McKee, R. W. (1956). The Inhibition of Respiration by Glucose, Fructose, and
771 Mannose in the Ehrlich Mouse Ascites Tumor. *Cancer Research*, *16*(4), 364–368.
772 Broach, J. R. (2012). Nutritional control of growth and development in yeast. *Genetics*,
773 *192*(1), 73–105. https://doi.org/10.1534/genetics.111.135731
774 Buchakjian, M. R., & Kornbluth, S. (2010). The engine driving the ship: Metabolic steering of
775 cell proliferation and death. *Nature Reviews Molecular Cell Biology*, *11*(10), 715–727.

776 https://doi.org/10.1038/nrm2972
777 Cai, L., & Tu, B. P. (2011). Driving the Cell Cycle Through Metabolism. *Annual Review of Cell*
778 *and Developmental Biology*, *28*(1), 59–87. https://doi.org/10.1146/annurev-cellbio-
779 092910-154010
780 Chen, W. W., Freinkman, E., & Sabatini, D. M. (2017). Rapid immunopurification of
781 mitochondria for metabolite profiling and absolute quantification of matrix
782 metabolites. *Nature Protocols*, *12*(10), 2215. https://doi.org/10.1038/NPROT.2017.104
783 Cheng, G., Zielonka, J., Dranka, B. P., McAllister, D., Mackinnon, A. C., Joseph, J., &
784 Kalyanaraman, B. (2012). Mitochondria-targeted drugs synergize with 2-deoxyglucose
785 to trigger breast cancer cell death. *Cancer Research*, *72*(10), 2634–2644.
786 https://doi.org/10.1158/0008-5472.CAN-11-3928/650337/AM/MITOCHONDRIA-
787 TARGETED-DRUGS-SYNERGIZE-WITH-2
788 Cornish-Bowden, A. (2016). Biochemical evolution : the pursuit of perfection. *Garland*
789 *Science*.
790 Crabtree, H. G. (1929). Observations on the carbohydrate metabolism of tumours.
791 *Biochemical Journal*, *23*(3), 536–545. https://doi.org/10.1042/bj0230536
792 De Deken, R. H. (1966). The Crabtree effect: a regulatory system in yeast. *Journal of General*
793 *Microbiology*, *44*(2), 149–156. https://doi.org/10.1099/00221287-44-2-149
794 Dechant, R., Binda, M., Lee, S. S., Pelet, S., Winderickx, J., & Peter, M. (2010). Cytosolic pH is
795 a second messenger for glucose and regulates the PKA pathway through V-ATPase.
796 *EMBO Journal*, *29*(15), 2515–2526. https://doi.org/10.1038/emboj.2010.138
797 Díaz-Ruiz, R., Avéret, N., Araiza, D., Pinson, B., Uribe-Carvajal, S., Devin, A., & Rigoulet, M.
798 (2008). Mitochondrial Oxidative Phosphorylation Is Regulated by Fructose 1,6-
799 Bisphosphate: A POSSIBLE ROLE IN CRABTREE EFFECT INDUCTION? *. *Journal of*
800 *Biological Chemistry*, *283*(40), 26948–26955. https://doi.org/10.1074/JBC.M800408200
801 Diaz-Ruiz, R., Rigoulet, M., & Devin, A. (2011). The Warburg and Crabtree effects: On the
802 origin of cancer cell energy metabolism and of yeast glucose repression. *Biochimica et*
803 *Biophysica Acta - Bioenergetics*, *1807*(6), 568–576.
804 https://doi.org/10.1016/j.bbabio.2010.08.010
805 Dicarlo, J. E., Norville, J. E., Mali, P., Rios, X., Aach, J., & Church, G. M. (2013). Genome
806 engineering in Saccharomyces cerevisiae using CRISPR-Cas systems. *Nucleic Acids*
807 *Research*, *41*(7), 4336–4343. https://doi.org/10.1093/NAR/GKT135

808 Fontanesi, F., Soto, I. C., Horn, D., & Barrientos, A. (2006). Assembly of mitochondrial
809 cytochrome c-oxidase, a complicated and highly regulated cellular process. *American*
810 *Journal of Physiology - Cell Physiology*, *291*(6), 1129–1147.
811 https://doi.org/10.1152/AJPCELL.00233.2006/ASSET/IMAGES/LARGE/ZH001106495400
812 05.JPEG
813 Gasmi, N., Jacques, P. E., Klimova, N., Guo, X., Ricciardi, A., Robert, F., & Turcotte, B. (2014).
814 The switch from fermentation to respiration in Saccharomyces cerevisiae is regulated
815 by the Ert1 transcriptional activator/repressor. *Genetics*, *198*(2), 547–560.
816 https://doi.org/10.1534/genetics.114.168609
817 Grigaitis, P., & Teusink, B. (2022). An excess of glycolytic enzymes under glucose-limited
818 conditions may enable Saccharomyces cerevisiae to adapt to nutrient availability. *FEBS*
819 *Letters*. https://doi.org/10.1002/1873-3468.14484
820 Gupta, R., & Laxman, S. (2021). Cycles, sources, and sinks: Conceptualizing how phosphate
821 balance modulates carbon flux using yeast metabolic networks. *ELife*, *10*, 1–14.
822 https://doi.org/10.7554/eLife.63341
823 Gupta, R., Walvekar, A. S., Liang, S., Rashida, Z., Shah, P., & Laxman, S. (2019). A tRNA
824 modification balances carbon and nitrogen metabolism by regulating phosphate
825 homeostasis. *ELife*, *8*, 1–33. https://doi.org/10.7554/eLife.44795
826 Hamel, P., Saint-Georges, Y., De Pinto, B., Lachacinski, N., Altamura, N., & Dujardin, G.
827 (2004). Redundancy in the function of mitochondrial phosphate transport in
828 Saccharomyces cerevisiae and Arabidopsis thaliana. *Molecular Microbiology*, *51*(2),
829 307–317. https://doi.org/10.1046/j.1365-2958.2003.03810.x
830 Hammad, N., Rosas-Lemus, M., Uribe-Carvajal, S., Rigoulet, M., & Devin, A. (2016). The
831 Crabtree and Warburg effects: Do metabolite-induced regulations participate in their
832 induction? *Biochimica et Biophysica Acta - Bioenergetics*, *1857*(8), 1139–1146.
833 https://doi.org/10.1016/j.bbabio.2016.03.034
834 Harden, A., & Young, W. J. (1908). The alcoholic Ferment of Yeast-juice.Part III.-The Function
835 of Phosphates in the Fermentation o f Glucose hy Yeast-juice. *Proceedings of the Royal*
836 *Society of London. Series B, 80*(540), 299–311. https://royalsocietypublishing.org/
837 Heiden, M. G. Vander, Cantley, L. C., & Thompson, C. B. (2009). Understanding the Warburg
838 Effect: The Metabolic Requirements of Cell Proliferation. *Science*, *324*(5930), 1029–
839 1033. https://doi.org/10.1126/science.1160809.Understanding

840 Hershko, A., & Ciechanover, A. (1998). THE UBIQUITIN SYSTEM. *Annual Review of*
841 *Biochemistry*, *67*, 425–479.
842 Hershko, A., Heller, H., Elias, S., & Ciechanover, A. (1983). Components of Ubiquitin-Protein
843 Ligase System. *The Journal of Biological Chemistry*, *258*(13), 8206–8214.
844 https://doi.org/papers2://publication/uuid/C82E58FF-33C7-42BF-BC20-CDD10219EC6E
845 Hitosugi, T., & Chen, J. (2014). Post-translational modifications and the Warburg effect.
846 *Oncogene*, *33*, 4279–4285. https://doi.org/10.1038/onc.2013.406
847 Hohmann, S., Bell, W., Neves, M. J., Valckx, D., & Thevelein, J. M. (1996). Evidence for
848 trehalose-6-phosphate-dependent and-independent mechanisms in the control of
849 sugar influx into yeast glycolysis. *Molecular Microbiology*, *20*(5), 981–991.
850 https://doi.org/10.1111/j.1365-2958.1996.tb02539.x
851 Hollinshead, W. D., Rodriguez, S., Martin, H. G., Wang, G., Baidoo, E. E. K., Sale, K. L.,
852 Keasling, J. D., Mukhopadhyay, A., & Tang, Y. J. (2016). Examining Escherichia coli
853 glycolytic pathways, catabolite repression, and metabolite channeling using Δpfk
854 mutants. *Biotechnology for Biofuels*, *9*(1), 1–13. https://doi.org/10.1186/s13068-016-
855 0630-y
856 Hunter, T. (2012). Why nature chose phosphate to modify proteins. *Philosophical*
857 *Transactions of the Royal Society B: Biological Sciences*, *367*(1602), 2513–2516.
858 https://doi.org/10.1098/RSTB.2012.0013
859 Isasa, M., Rose, C. M., Elsasser, S., Navarrete-Perea, J., Paulo, J. A., Finley, D. J., & Gygi, S. P.
860 (2015). Multiplexed, Proteome-Wide Protein Expression Profiling: Yeast
861 Deubiquitylating Enzyme Knockout Strains. *Journal of Proteome Research*, *14*(12),
862 5306–5317. https://doi.org/10.1021/acs.jproteome.5b00802
863 J.P. van Dijken, J. B., Brambillac, L., Dubocd, P., Francoise, J. M., Gancedof, C., Giusepping,
864 M.L.F.HEijnenh, J. J., Hoarei, M., Langej, H. C., Maddenk, E. A., Niederbergerb, P.,
865 Nielsend, J., J.L. Parroue , T. Petitf , D. Porroc, M. R., Rielg, N. van, Rizzij, M., & H.Y.
866 Steensmaa, k , C.T. Verripsg, J. Vindeløvd, Pronka, J. T. (2000). An interlaboratory
867 comparison of physiological and genetic properties of four Saccharomyces cerevisiae
868 strains. *Enzyme and Microbial Technology*, *26*, 706–714.
869 Jia, F., Wan, X., Zhu, W., Sun, D., Zheng, C., Liu, P., & Huang, J. (2015). Overexpression of
870 Mitochondrial Phosphate Transporter 3 Severely Hampers Plant Development through
871 Regulating Mitochondrial Function in Arabidopsis. *PLOS ONE*, *10*(6), e0129717.

https://doi.org/10.1371/JOURNAL.PONE.0129717

Kamerlin, S. C. L., Sharma, P. K., Prasad, R. B., & Warshel, A. (2013). Why nature really chose phosphate. *Quarterly Reviews of Biophysics*, *46*(1), 1–132. https://doi.org/10.1017/S0033583512000157

Komander, D., & Rape, M. (2012). The Ubiquitin Code. *Annual Review of Biochemistry*, *81*(1), 203–229. https://doi.org/10.1146/annurev-biochem-060310-170328

Koobs, D. H. (1972). Phosphate mediation of the Crabtree and Pasteur effects. *Science*, *178*(4057), 127–133. https://doi.org/10.1126/science.178.4057.127

Kornberg, M. D. (2020). The immunologic Warburg effect: Evidence and therapeutic opportunities in autoimmunity. *Wiley Interdisciplinary Reviews: Systems Biology and Medicine*, *12*(5), 1–17. https://doi.org/10.1002/wsbm.1486

Laussel, C., & Léon, S. (2020). Cellular toxicity of the metabolic inhibitor 2-deoxyglucose and associated resistance mechanisms. *Biochemical Pharmacology*, *182*, 114213. https://doi.org/10.1016/J.BCP.2020.114213

Lemus, M. R., Roussarie, E., Hammad, N., Mougeolle, A., Ransac, S., Issa, R., Mazat, J. P., Uribe-Carvajal, S., Rigoulet, M., & Devin, A. (2018). The role of glycolysis-derived hexose phosphates in the induction of the Crabtree effect. *Journal of Biological Chemistry*, *293*(33), 12843–12854. https://doi.org/10.1074/JBC.RA118.003672

Liao, P. C., Boldogh, I. R., Siegmund, S. E., Freyberg, Z., & Pon, L. A. (2018). Isolation of mitochondria from Saccharomyces cerevisiae using magnetic bead affinity purification. *PLoS ONE*, *13*(4), 1–15. https://doi.org/10.1371/journal.pone.0196632

Ljungdahl, P. O., & Daignan-Fornier, B. (2012). Regulation of amino acid, nucleotide, and phosphate metabolism in Saccharomyces cerevisiae. *Genetics*, *190*(3), 885–929. https://doi.org/10.1534/genetics.111.133306

Longtine, M. S., McKenzie, A., Demarini, D. J., Shah, N. G., Wach, A., Brachat, A., Philippsen, P., & Pringle, J. R. (1998). Additional modules for versatile and economical PCR-based gene deletion and modification in Saccharomyces cerevisiae. *Yeast*, *14*(10), 953–961. https://doi.org/10.1002/(SICI)1097-0061(199807)14:10<953::AID-YEA293>3.0.CO;2-U

López-lázaro, M. (2008). *The Warburg Effect : Why and How do Cancer Cells Activate Glycolysis in the Presence of Oxygen ?* 305–312.

Lu, C. L., Qin, L., Liu, H. C., Candas, D., Fan, M., & Li, J. J. (2015). Tumor Cells Switch to Mitochondrial Oxidative Phosphorylation under Radiation via mTOR-Mediated

Hexokinase II Inhibition - A Warburg-Reversing Effect. *PLOS ONE*, *10*(3), e0121046. https://doi.org/10.1371/JOURNAL.PONE.0121046

Mason, P. W., Carbone, D. P., Cushman, R. A., & Waggoner, A. S. (1981). The importance of inorganic phosphate in regulation of energy metabolism of Streptococcus lactis. *Journal of Biological Chemistry*, *256*(4), 1861–1866. https://doi.org/10.1016/S0021-9258(19)69886-8

McCommis, K. S., & Finck, B. N. (2015). Mitochondrial pyruvate transport: a historical perspective and future research directions. *The Biochemical Journal*, *466*(3), 443. https://doi.org/10.1042/BJ20141171

Miyazawa, H., Yamaguchi, Y., Sugiura, Y., Honda, K., Kondo, K., Matsuda, F., Yamamoto, T., Suematsu, M., & Miura, M. (2017). Rewiring of embryonic glucose metabolism via suppression of PFK-1 and aldolase during mouse chorioallantoic branching. *Development (Cambridge)*, *144*(1), 63–73. https://doi.org/10.1242/dev.138545

Mouillon, J. M., & Persson, B. L. (2006). New aspects on phosphate sensing and signalling in Saccharomyces cerevisiae. *FEMS Yeast Research*, *6*(2), 171–176. https://doi.org/10.1111/j.1567-1364.2006.00036.x

Murakami, H., Blobel, G., & Pain, D. (1990). Isolation and characterization of the gene for a yeast mitochondrial import receptor. *Nature 1990 347:6292*, *347*(6292), 488–491. https://doi.org/10.1038/347488a0

Nelson, D. L. (David L., Nelson, D. L. (David L., Lehninger, A. L., & Cox, M. M. (2008). *Lehninger principles of biochemistry*. https://books.google.com/books/about/Lehninger_Principles_of_Biochemistry.html?id=fg9PPgAACAAJ

Nostramo, R., Varia, S. N., Zhang, B., Emerson, M. M., & Herman, P. K. (2016). The Catalytic Activity of the Ubp3 Deubiquitinating Protease Is Required for Efficient Stress Granule Assembly in Saccharomyces cerevisiae. *Molecular and Cellular Biology*, *36*(1), 173. https://doi.org/10.1128/MCB.00609-15

O'Neill, S., Porter, R. K., McNamee, N., Martinez, V. G., & O'Driscoll, L. (2019). 2-Deoxy-D-Glucose inhibits aggressive triple-negative breast cancer cells by targeting glycolysis and the cancer stem cell phenotype. *Scientific Reports*, *9*(1), 1–11. https://doi.org/10.1038/s41598-019-39789-9

Oliveira, G. L., Coelho, A. R., Marques, R., & Oliveira, P. J. (2021). Cancer cell metabolism:

Rewiring the mitochondrial hub. *Biochimica et Biophysica Acta - Molecular Basis of Disease*, *1867*(2), 166016. https://doi.org/10.1016/j.bbadis.2020.166016

Orij, R., Brul, S., & Smits, G. J. (2011). Intracellular pH is a tightly controlled signal in yeast. *Biochimica et Biophysica Acta - General Subjects*, *1810*(10), 933–944. https://doi.org/10.1016/j.bbagen.2011.03.011

Ossareh-Nazari, B., Bonizec, M., Cohen, M., Dokudovskaya, S., Delalande, F., Schaeffer, C., Van Dorsselaer, A., & Dargemont, C. (2010). Cdc48 and Ufd3, new partners of the ubiquitin protease Ubp3, are required for ribophagy. *EMBO Reports*, *11*(7), 548–554. https://doi.org/10.1038/embor.2010.74

Pacini, N., & Borziani, F. (2014). Cancer stem cell theory and the warburg effect, two sides of the same Coin? *International Journal of Molecular Sciences*, *15*(5), 8893–8930. https://doi.org/10.3390/ijms15058893

Pelicano, H., Martin, D. S., Xu, R. H., & Huang, P. (2006). Glycolysis inhibition for anticancer treatment. *Oncogene 2006 25:34*, *25*(34), 4633–4646. https://doi.org/10.1038/sj.onc.1209597

Pickart, C. M., & Eddins, M. J. (2004). Ubiquitin: Structures, functions, mechanisms. *Biochimica et Biophysica Acta - Molecular Cell Research*, *1695*(1–3), 55–72. https://doi.org/10.1016/j.bbamcr.2004.09.019

Poncet, D., Pauleau, A. L., Szabadkai, G., Vozza, A., Scholz, S. R., Le Bras, M., Brière, J. J., Jalil, A., Le Moigne, R., Brenner, C., Hahn, G., Wittig, I., Schägger, H., Lemaire, C., Bianchi, K., Souquère, S., Pierron, G., Rustin, P., Goldmacher, V. S., … Kroemer, G. (2006). Cytopathic effects of the cytomegalovirus-encoded apoptosis inhibitory protein vMIA. *Journal of Cell Biology*, *174*(7), 985–996. https://doi.org/10.1083/jcb.200604069

Postma, E., Verduyn, C., Scheffers, W. A., & Van Dijken, J. P. (1989). Enzymic analysis of the crabtree effect in glucose-limited chemostat cultures of Saccharomyces cerevisiae. *Applied and Environmental Microbiology*, *55*(2), 468–477. http://www.ncbi.nlm.nih.gov/pubmed/2566299%0Ahttp://www.pubmedcentral.nih.gov/articlerender.fcgi?artid=PMC184133

Rodríguez-Enríquez, S., Juárez, O., Rodríguez-Zavala, J. S., & Moreno-Sánchez, R. (2001). Multisite control of the Crabtree effect in ascites hepatoma cells. *European Journal of Biochemistry*, *268*(8), 2512–2519. https://doi.org/10.1046/j.1432-1327.2001.02140.x

Scheibye-Knudsen, M., & Quistorff, B. (2009). Regulation of mitochondrial respiration by

968 inorganic phosphate; comparing permeabilized muscle fibers and isolated
969 mitochondria prepared from type-1 and type-2 rat skeletal muscle. *European Journal of*
970 *Applied Physiology*, *105*(2), 279–287. https://doi.org/10.1007/s00421-008-0901-9
971 Secco, D., Wang, C., Shou, H., & Whelan, J. (2012). Phosphate homeostasis in the yeast
972 Saccharomyces cerevisiae, the key role of the SPX domain-containing proteins. *FEBS*
973 *Letters*, *586*(4), 289–295. https://doi.org/10.1016/j.febslet.2012.01.036
974 Seifert, E. L., Ligeti, E., Mayr, J. A., Sondheimer, N., & Hajnóczky, G. (2015). The
975 mitochondrial phosphate carrier: Role in oxidative metabolism, calcium handling and
976 mitochondrial disease. *Biochemical and Biophysical Research Communications*, *464*(2),
977 369–375. https://doi.org/10.1016/J.BBRC.2015.06.031
978 Shestov, A. A., Liu, X., Ser, Z., Cluntun, A. A., Hung, Y. P., Huang, L., Kim, D., Le, A., Yellen, G.,
979 Albeck, J. G., & Locasale, J. W. (2014). Quantitative determinants of aerobic glycolysis
980 identify flux through the enzyme GAPDH as a limiting step. *ELife*, *3*(July2014), 1–18.
981 https://doi.org/10.7554/ELIFE.03342
982 Shiratori, R., Furuichi, K., Yamaguchi, M., Miyazaki, N., Aoki, H., Chibana, H., Ito, K., & Aoki, S.
983 (2019). Glycolytic suppression dramatically changes the intracellular metabolic profile
984 of multiple cancer cell lines in a mitochondrial metabolism-dependent manner.
985 *Scientific Reports*, *9*(1), 1–15. https://doi.org/10.1038/s41598-019-55296-3
986 Solesio, M. E., Xie, L., McIntyre, B., Ellenberger, M., Mitaishvili, E., Bhadra-Lobo, S., Bettcher,
987 L. F., Bazil, J. N., Raftery, D., Jakob, U., & Pavlov, E. V. (2021). Depletion of
988 mitochondrial inorganic polyphosphate (polyP) in mammalian cells causes metabolic
989 shift from oxidative phosphorylation to glycolysis. *Biochemical Journal*, *478*(8), 1631–
990 1646. https://doi.org/10.1042/BCJ20200975
991 Soto-Heredero, G., Gómez de las Heras, M. M., Gabandé-Rodríguez, E., Oller, J., &
992 Mittelbrunn, M. (2020). Glycolysis – a key player in the inflammatory response. *The*
993 *FEBS Journal*, *287*(16), 3350–3369. https://doi.org/10.1111/FEBS.15327
994 Sriariyanun, M., Mutrakulcharoen, P., Tepaamorndech, S., Cheenkachorn, K., & Rattanaporn,
995 K. (2019). A Rapid Spectrophotometric Method for Quantitative Determination of
996 Ethanol in Fermentation Products. *Oriental Journal of Chemistry*, *35*(2), 744–750.
997 https://doi.org/10.13005/OJC/350234
998 Sussman, I., Erecińska, M., & Wilson, D. F. (1980). Regulation of cellular energy metabolism.
999 The Crabtree effect. *Biochimica et Biophysica Acta - Bioenergetics*, *591*(2), 209–223.

https://doi.org/10.1016/0005-2728(80)90153-X

Timoń-Gómez, A., Proft, M., & Pascual-Ahuir, A. (2013). Differential Regulation of Mitochondrial Pyruvate Carrier Genes Modulates Respiratory Capacity and Stress Tolerance in Yeast. *PLOS ONE*, *8*(11), e79405. https://doi.org/10.1371/JOURNAL.PONE.0079405

Tripodi, F., Nicastro, R., Reghellin, V., & Coccetti, P. (2015). Post-translational modifications on yeast carbon metabolism: Regulatory mechanisms beyond transcriptional control. *Biochimica et Biophysica Acta - General Subjects*, *1850*(4), 620–627. https://doi.org/10.1016/j.bbagen.2014.12.010

Tsogtbaatar, E., Landin, C., Minter-Dykhouse, K., & Folmes, C. D. L. (2020). Energy Metabolism Regulates Stem Cell Pluripotency. *Frontiers in Cell and Developmental Biology*, *8*(February), 1–16. https://doi.org/10.3389/fcell.2020.00087

Van Heerden, J. H., Wortel, M. T., Bruggeman, F. J., Heijnen, J. J., Bollen, Y. J. M., Planqué, R., Hulshof, J., O'Toole, T. G., Wahl, S. A., & Teusink, B. (2014). Lost in transition: Start-up of glycolysis yields subpopulations of nongrowing cells. *Science*, *343*(6174). https://doi.org/10.1126/SCIENCE.1245114

Vengayil, V., Rashida, Z., & Laxman, S. (2019). The E3 ubiquitin ligase Pib1 regulates effective gluconeogenic shutdown upon glucose availability. *Journal of Biological Chemistry*, *294*(46), 17209–17223. https://doi.org/10.1074/JBC.RA119.009822/ATTACHMENT/D1BC32BA-1F6B-409C-A695-781AB3567758/MMC1.ZIP

Vila, T., Frases, S., & Gomesid, F. M. (2022). Lessons from protozoans: Phosphate sensing and polyphosphate storage in fungi. *PLOS Pathogens*, *18*(3), e1010298. https://doi.org/10.1371/JOURNAL.PPAT.1010298

Walvekar, A., Rashida, Z., Maddali, H., & Laxman, S. (2018). *A versatile LC-MS / MS approach for comprehensive , quantitative analysis of central metabolic pathways [version 1 ; peer review : 2 approved]*. *Sep*, 1–15.

Warburg, O. (1925). The metabolism of carcinoma cells 1. *The Journal of Cancer Research*, *9*(1), 148–163. https://doi.org/10.1158/jcr.1925.148

Westheimer, F. H. (1987). Why Nature Chose Phosphates. *Science*, *235*(4793), 1173–1178. https://doi.org/10.1126/SCIENCE.2434996

Wu, R., & Racker, E. (1959). Regulatory Mechanisms in Carbohydrate Metabolism. *Journal of*

1032 *Biological Chemistry*, *234*(5), 1036–1041. https://doi.org/10.1016/s0021-
1033 9258(18)98125-1
1034 Xia, L., Oyang, L., Lin, J., Tan, S., Han, Y., Wu, N., Yi, P., Tang, L., Pan, Q., Rao, S., Liang, J.,
1035 Tang, Y., Su, M., Luo, X., Yang, Y., Shi, Y., Wang, H., Zhou, Y., & Liao, Q. (2021). The
1036 cancer metabolic reprogramming and immune response. *Molecular Cancer*, *20*(1), 1–
1037 21. https://doi.org/10.1186/s12943-021-01316-8
1038 Yi, W., Clark, P. M., Mason, D. E., Keenan, M. C., Hill, C., Goddard, W. A., Peters, E. C.,
1039 Driggers, E. M., & Hsieh-Wilson, L. C. (2012). PFK1 Glycosylation Is a Key Regulator of
1040 Cancer Cell Growth and Central Metabolic Pathways. *Science (New York, N.Y.)*,
1041 *337*(6097), 975. https://doi.org/10.1126/SCIENCE.1222278
1042 Yoshikawa, S., Shinzawa-Itoh, K., Nakashima, R., Yaono, R., Yamashita, E., Inoue, N., Yao, M.,
1043 Fei, M. J., Libeu, C. P., Mizushima, T., Yamaguchi, H., Tomizaki, T., & Tsukihara, T.
1044 (1998). Redox-coupled crystal structural changes in bovine heart cytochrome c oxidase.
1045 *Science*, *280*(5370), 1723–1729. https://doi.org/10.1126/science.280.5370.1723
1046 Zara, V., Dietmeier, K., Palmisano, A., Vozza, A., Rassow, J., Palmieri, F., & Pfanner, N. (1996).
1047 Yeast mitochondria lacking the phosphate carrier/p32 are blocked in phosphate
1048 transport but can import preproteins after regeneration of a membrane potential.
1049 *Molecular and Cellular Biology*, *16*(11), 6524–6531.
1050 https://doi.org/10.1128/mcb.16.11.6524
1051 Zhu, J., & Thompson, C. B. (2019). Metabolic regulation of cell growth and proliferation.
1052 *Nature Reviews Molecular Cell Biology*, *20*(7), 436–450.
1053 https://doi.org/10.1038/s41580-019-0123-5
1054
1055

1056 **Figure legends**

1057 **Figure 1: A deubiquitinase deletion screen identifies Ubp3 as a regulator of glucose-**
1058 **mediated mitochondrial repression**

1059 A) Schematic depicting glucose-mediated mitochondrial repression (Crabtree effect).
1060 Crabtree positive cells have high fermentation and repressed mitochondrial activity in high
1061 glucose.

1062 B) Schematic describing the screen with a yeast library with individual knock-outs of
1063 deubiquitinase enzymes (DUBs), to identify regulators of glucose-mediated mitochondrial
1064 repression.

1065 C) Identifying DUB deficient cells with altered mitochondrial potential. The heat map shows
1066 the relative mitochondrial membrane potential of 19 deubiquitinase deletion mutants in high
1067 glucose. The cells were grown in high (2%) glucose, stained with mitotracker CMXRos and
1068 fluorescence intensity measured. Mean mitotracker intensity obtained from 2 biological
1069 replicates is shown in the heatmap. Also see supplementary figure S1A, S1B.

1070 D) The deubiquitinase activity of Ubp3 and glucose-mediated repression of mitochondrial
1071 membrane potential. A catalytically inactive mutant of Ubp3, $Ubp3^{C469A}$ was generated. WT,
1072 *ubp3Δ,* and $Ubp3^{C469A}$ cells were grown in high glucose and the relative mitochondrial
1073 membrane potential was measured. Data represent mean ± SD (n=3). Also see supplementary
1074 figure S1D.

1075 E) Effect of loss of Ubp3 on the electron transport chain complex IV subunit protein Cox2. WT
1076 and *ubp3Δ* cells were grown in high glucose and Cox2 protein was measured by western blot
1077 using an anti-Cox2 antibody. A representative blot (out of 3 biological replicates, n=3) is
1078 shown in the panel.

1079 F) Basal oxygen consumption rate (OCR) in high glucose in *ubp3Δ* cells. WT and *ubp3Δ* cells
1080 were grown in high glucose medium and the basal OCR was measured using a seahorse XFe24
1081 analyzer. Sodium azide (complex IV inhibitor) injection was done after three basal OCR
1082 measurements to estimate the non-mitochondrial respiration. Basal OCR corresponding to ~3

1083 x 10^5 cells, from two independent experiments (n=2), normalized to the OD_{600} is shown. Bar
1084 graph representations of the data are shown in the inset.

1085 G) Total ATP levels in *ubp3Δ* and WT cells. WT and *ubp3Δ* cells were grown in high glucose
1086 medium, and the total ATP were measured. Data represent mean ± SD (n=3).

1087 H) Dependence of *ubp3Δ* cells on mitochondrial ATP. WT and *ubp3Δ* cells were grown in high
1088 glucose medium, and treated with 1 mM sodium azide for 45 minutes. The total ATP levels in
1089 sodium azide treated and untreated cells were measured. Data represent mean ± SD (n=3).

1090 I) Requirement for mitochondrial respiration in high glucose in *ubp3Δ* cells. Serial dilution
1091 growth assay in high glucose in the presence and absence of ETC complex IV inhibitor sodium
1092 azide (1 mM) are shown. Also see supplementary figure S1F.

1093 The Coomassie-stained gel for total protein was used as a loading control for all western blots.
1094 All western blot quantifications were done using ImageJ software. The graphs were plotted
1095 using GraphPad prism 9.0.1. The statistical significance was calculated using an unpaired-
1096 student t-test. *p<0.05, **p<0.01, ***p<0.001.

1097

1098 **Figure 2: Key glycolytic enzymes decrease and glucose flux is rerouted in *ubp3Δ* cells**

1099 A) A schematic illustrating directions of glucose-6-phosphate (G6)) flux in cells. Glucose is
1100 converted to G6P, which is a precursor for trehalose, the pentose phosphate pathway (PPP),
1101 and glycolysis. In high glucose, *S. cerevisiae* cells have high glycolysis, and pyruvate is
1102 converted to ethanol (fermentation). Phosphofructokinase 1 (Pfk1) catalyzes the conversion
1103 of fructose-6 phosphate (F6P) to fructose-1,6 bisphosphate (F1,6 BP) which is the committed
1104 step of glycolysis. F1,6 BP is converted to glyceraldehyde-3 phosphate (G3P) which is then
1105 converted to 1,3 bisphosphoglycerate (1,3 BPG) by the enzyme glyceraldehyde phosphate
1106 dehydrogenase (GAPDH). Two major isozymes of GAPDH in yeast- Tdh2 and Tdh3 are shown
1107 in the schematic.

1108 B) Effect of loss of Ubp3 on key glycolytic enzymes. WT and *ubp3Δ* cells containing epitope
1109 tagged Pfk1, Tdh2, and Tdh3 were grown in high glucose and the protein levels were

1110 measured by western blot using an anti-FLAG antibody. A representative blot (out of n=3) is
1111 shown. Also see supplementary figure S2A.

1112 C) Steady-state metabolite amounts in WT and *ubp3Δ* cells in high glucose. The relative
1113 steady-state levels of trehalose, major glycolytic, and PPP intermediates were estimated using
1114 targeted LC-MS/MS in WT and *ubp3Δ* cells grown in high glucose. Data represent mean ± SD
1115 (n=3). Also see table S3.

1116 D) Relative glycolytic and trehalose synthesis flux in WT and *ubp3Δ* cells. The relative ^{13}C label
1117 incorporation into trehalose and glycolytic intermediates, after a pulse of 1% $^{13}C_6$ glucose is
1118 shown. Data represent mean ± SD (n=3). Also see table S3, figures S2B, S2C.

1119 E) Ethanol production in *ubp3Δ* cells. WT and *ubp3Δ* cells were grown in high glucose and the
1120 ethanol concentration in the media was measured. Data represent mean ± SD (n=3).

1121 F) Relative rate of ethanol production in WT vs *ubp3Δ* cells. WT and *ubp3Δ* cells were grown
1122 in high glucose and at OD_{600} ~ 0.6, equal number of cells were shifted to fresh medium (high
1123 glucose) and the ethanol concentration in the medium was measured temporally. Data
1124 represent mean ± SD (n=3)

1125 Statistical significance was calculated using unpaired-student t-test. *p<0.05, **p<0.01,
1126 ***p<0.001.

1127

1128 **Figure 3: Phosphate (Pi) accumulates due to altered Pi homeostasis in *ubp3Δ* cells**

1129 A) Schematic showing the maintenance of Pi balance during glycolysis. Trehalose synthesis
1130 from G6P releases free Pi, and the conversion of G3P to 1,3BPG by GAPDH is a major Pi
1131 consumer. This balance between Pi release and consumption maintains cytosolic Pi levels. In
1132 *ubp3Δ* cells, there is an increase in trehalose biosynthesis (which releases Pi). *ubp3Δ* cells have
1133 decreased GAPDH, which will decrease Pi consumption. This increase in Pi release along with
1134 a decrease in Pi consumption could increase cytosolic Pi.

1135 B) Intracellular Pi levels in WT and *ubp3Δ* cells. WT and *ubp3Δ* cells were grown in high glucose
1136 and the total free phosphate (Pi) levels were estimated. WT cells grown in high Pi (2% glucose,

1137 10mM Pi) was used as the positive control. Data represent mean ± SD (n=3). Also see
1138 supplementary figure S3A.

1139 C) Pho regulon responses in WT and *ubp3Δ* cells. Protein levels of Pho84-FLAG and Pho12-
1140 FLAG were compared between WT cells grown in high glucose and in high Pi, *ubp3Δ* cells in
1141 high glucose with or without a shift to a no-Pi medium for one hour, by western blot using an
1142 anti-FLAG antibody. A representative blot (out of n=3) is shown.

1143 D) Contribution of trehalose synthesis as a Pi source in *ubp3Δ* cells. WT, *tps2Δ*, *ubp3Δ,* and
1144 *ubp3Δtps2Δ* cells were grown in high glucose and the total Pi levels were estimated by
1145 malachite green assay. Data represent mean ± SD (n=3). Also see supplementary figure S3B.

1146 E) Loss of GAPDH isozymes Tdh2 and Tdh3 and effect on Pi levels. WT, *ubp3Δ,* and *tdh2Δtdh3Δ*
1147 cells were grown in high glucose and the total Pi levels were estimated. Data represent mean
1148 ± SD (n=3). Also see supplementary figure S3F.

1149 The statistical significance was calculated using unpaired-student t-test. *p<0.05, **p<0.01,
1150 ***p<0.001.

1151

1152 **Figure 4: Phosphate availability dictates mitochondrial activity**

1153 A) Schematic depicting a hypothetical mechanism of cytosolic free Pi controling mitochondrial
1154 activity by regulating mitochondrial Pi availability. In *ubp3Δ* cells, the increased Pi release
1155 coupled with the decreased Pi consumption results in increasing Pi, which can increase the Pi
1156 available for transport to mitochondria and enhance mitochondrial activity.

1157 B) Mitochondrial Pi amounts in WT vs *ubp3Δ* cells. Mitochondria were isolated by
1158 immunoprecipitation from WT and *ubp3Δ* cells and mitochondrial Pi was estimated. The Pi
1159 levels in mitochondria, normalised to Idh1 protein levels are shown. Data represent mean ±
1160 SD (n=3). Also see supplementary figure S4A, B.

1161 C) Cox2 protein in *tdh2Δtdh3Δ* cells. WT, *ubp3Δ,* and *tdh2Δtdh3Δ* cells were grown in high
1162 glucose and Cox2 protein was estimated by western blot. A representative blot (out of n=3)
1163 is shown in the panel.

1164 D) Basal OCR levels in high glucose in *tdh2Δtdh3Δ* cells. WT, *ubp3Δ,* and *tdh2Δtdh3Δ* cells were
1165 grown in high glucose and the basal OCR was measured from two independent experiments
1166 (n=2). Also see supplementary figure S4C.

1167 E) Pi amounts and Cox2 protein levels in *ubp3Δ* and *tdh2Δtdh3Δ* vs WT cells. WT cells were
1168 grown in high glucose, *ubp3Δ* and *tdh2Δtdh3Δ* cells were grown in high glucose and low Pi
1169 medium, and Cox2 protein was estimated by western blot. A representative blot (n=3) is
1170 shown. Also see supplementary figure S4D, S4F.

1171 F) Pi amounts and basal OCR in *ubp3Δ* and *tdh2Δtdh3Δ* vs WT cells. WT cells were grown in
1172 high glucose, *ubp3Δ* and *tdh2Δtdh3Δ* cells were grown in high glucose and low Pi medium,
1173 and the basal OCR was measured from two independent experiments (n=2).

1174 G) Effect of loss of mitochondrial Pi transporter Mir1 on Cox2 protein. WT, *ubp3Δ*, *mir1Δ,* and
1175 *mir1Δubp3Δ* cells were grown in high glucose and Cox2 protein was estimated by western
1176 blot. A representative blot (n=3) is shown.

1177 H) Relationship of mitochondrial Pi transport and basal OCR in WT vs *ubp3Δ* cells. WT, *ubp3Δ*,
1178 *mir1Δ,* and *mir1Δubp3Δ* cells were grown in high glucose and the basal OCR was measured
1179 from two independent experiments (n=2).

1180 The statistical significance was calculated using unpaired-student t-test. *$p<0.05$, **$p<0.01$,
1181 ***$p<0.001$.

1182

1183 **Figure 5: Mitochondrial Pi availability controls glucose-mediated mitochondrial repression**.

1184 A) Relationship of mitochondrial Pi transport and respiration after glucose removal. WT and
1185 *mir1Δ* cells were cultured in high glucose (2% glucose) and shifted to low (0.1%) glucose for 1
1186 hour. The basal OCR with and without a shift to low glucose was measured. The basal OCR
1187 corresponding to ~3 x 10^5 cells, normalized to the OD_{600}, from two independent experiments
1188 (n=2) are shown.

1189 B) Requirement of mitochondrial Pi transport for cells to switch to respiration upon glycolytic
1190 inhibition by 2DG. WT and *mir1Δ* cells were cultured in high glucose and treated with or

1191 without 0.25% 2DG for 1 hour. The basal OCR was measured from two independent
1192 experiments (n=2). Also see supplementary figure S5A.

1193 C) Glucose-dependent regulation of the mitochondrial Pi transporter Mir1. Cells containing
1194 endogenous Mir1 chromosomally tagged at the C terminus with a 6x HA epitope tag were
1195 grown in a high glucose and shifted to low glucose (0.1% glucose) for 1 hour. The protein
1196 levels of Mir1 were estimated and compared. A representative blot (out of n=3) is shown in
1197 the panel. Also see supplementary figure S5B.

1198 D) Increasing Pi concentrations and mitochondrial activity in isolated mitochondria.
1199 Mitochondria were isolated from WT cells grown in high glucose, incubated with 1 mM
1200 pyruvate, 1 mM malate, 0.5 mM ADP and 0-50 mM KH_2PO_4. The mitochondrial activity was
1201 estimated by measuring mitotracker fluorescence intensity, and relative intensities
1202 normalised to the sample with 0 mM KH_2PO_4 is shown. Data represent mean ± SD (n=3).

1203 E) Effect of overexpressing Mir1 on Cox2 protein. Mir1-HA was overexpressed under a G6PD
1204 promoter. WT (containing empty vector) and Mir1 overexpressing (Mir1 OE) cells were grown
1205 in high glucose and Cox2 protein was estimated by western blot. A representative blot (out
1206 of n=3) is shown in the panel. Also see supplementary figure S5F.

1207 F) Effect of overexpressing Mir1 on basal OCR. WT (containing empty vector) and Mir1 OE
1208 cells were grown in high glucose medium, and the basal OCR was measured from two
1209 independent experiments (n=3).

1210 G) Mitochondrial Pi transport requirement for growth after 2DG treatment. Shown are serial
1211 dilution growth assays in high glucose in the presence and absence of 0.1% 2DG, using WT
1212 and *mir1Δ* cells. The results after 40hrs incubation at 30°C are shown.

1213 I) A model illustrating how Pi availability to the mitochondria controls mitochondrial activity.
1214 In high glucose, the decreased Pi due to high Pi consumption in glycolysis, along with the
1215 glucose-mediated repression of mitochondrial Pi transporters, results in decreased
1216 mitochondrial Pi availability. This results in reduced mitochondrial activity. In low glucose,
1217 increased mitochondrial Pi transporters (and lower glycolytic flux) increases the
1218 mitochondrial Pi, leading to enhanced mitochondrial activity. In *ubp3Δ* cells in high glucose,

1219 high trehalose synthesis and lower glycolytic flux results in an increase in Pi levels. This
1220 increases the mitochondrial Pi availability and thereby increases the mitochondrial activity.

1221 The statistical significance was calculated using unpaired-student t-test. *p<0.05, **p<0.01,
1222 ***p<0.001.

1223

1224 **Supplement figures:**

1225 **Figure S1:**

1226 A) A list of the known/identified *S. cerevisiae* deubiquitinase enzymes is shown. The DUBs
1227 which were used in this study, and the mitotracker intensity of two biological replicates (n=2)
1228 relative to WT are shown.

1229 B) WT cells grown in a respiratory, ethanol medium and mitotracker fluorescence intensity
1230 compared to glucose medium. WT cells were grown in high glucose medium (2% glucose) and
1231 ethanol medium (2% ethanol), and the mitochondrial membrane potential was measured.
1232 Data from two independent experiments (n=2) is shown.

1233 C) Schematic representation of the conserved domains of Ubp3 and its mammalian ortholog
1234 Usp10. The catalytic cysteine of Usp10 and Ubp3 is highlighted.

1235 D) The catalytically inactive mutant of Ubp3, $Ubp3^{C469A}$ does not have altered Ubp3 protein
1236 levels. WT and $Ubp3^{C469A}$ cells containing endogenous Ubp3 tagged with 3xFLAG (C terminus)
1237 were grown in high glucose and the protein levels of Ubp3 were measured. A representative
1238 blot (n=3) is shown in the panel.

1239 E) Tom70 protein amounts do not change in *ubp3Δ* cells. WT and *ubp3Δ* cells containing
1240 endogenous Tom70 tagged at the C terminus with a 3xFLAG epitope were grown in high
1241 glucose and the protein levels of Tom70 were measured by western blot. A representative
1242 blot (n=3) is shown.

1243 F) Loss of proteins regulating mitochondrial respiration and growth defects in *ubp3Δ* cells in
1244 high glucose. Serial dilution growth assay was done in high glucose. The results after 24 hours
1245 of incubation at 30°C are shown.

1246 The statistical significance was calculated using unpaired-student t-test. *p<0.05, **p<0.01,
1247 ***p<0.001.

1248

1249 **Figure S2:**

1250 A) Loss of Ubp3 does not change the protein levels of enolase isozymes Eno1 and Eno2. WT
1251 and *ubp3Δ* cells containing Eno1 and Eno2 C terminus endogenously tagged with a 3x FLAG
1252 epitope, were grown in high glucose and protein amounts were estimated. A representative
1253 blot (out of n=3) is shown in the panel.

1254 B) Schematic showing the experimental design for measuring ^{13}C label incorporation into
1255 glycolytic intermediates and trehalose using a $^{13}C_6$ glucose-pulse.

1256 C) Changes in ^{13}C label incorporation into glycolytic intermediates and trehalose with time,
1257 and linearity of label incorporation after a pulse of 1% $^{13}C_6$ glucose is shown.

1258 The statistical significance was calculated using unpaired-student t-test. *p<0.05, **p<0.01,
1259 ***p<0.001.

1260

1261 **Figure S3:**

1262 A) Loss of Ubp3 deubiquitinase activity and Pi levels. WT, *ubp3Δ,* and Ubp3^{C469A} cells were
1263 grown in high glucose and the total free phosphate (Pi) levels were estimated. Data from two
1264 independent experiments (n=2) is shown.

1265 B) Trehalose levels in WT and *ubp3Δ* cells in the absence of Tps2. *tps2Δ* and *ubp3Δtps2Δ* cells
1266 were grown in high glucose, and the trehalose levels were estimated using targeted LC-
1267 MS/MS. Data represent mean ± SD (n=3).

1268 C) Loss of GAPDH isozymes Tdh2 and Tdh3 and ethanol production. WT and *tdh2Δtdh3Δ* cells
1269 were grown in high glucose and the ethanol concentration in the medium was measured.
1270 Data are represented as mean ± SD (n=3). Note: The WT shown here is same as the WT in
1271 Figure 2E, since the ethanol assays in Figure 2E and Figure S3C were done together and the
1272 common WT control was used.

1273 D) Steady state levels of glycolytic intermediates: *tdh2Δtdh3Δ* cells have unaltered steady
1274 state levels of G6P/F6P, increased levels of F1,6 BP and G3P and decreased levels of 3PG and
1275 PEP. WT and *tdh2Δtdh3Δ* cells were grown in high glucose and the steady state amounts of
1276 glycolytic intermediates were estimated using targeted LC-MS/MS. Data represent mean ± SD
1277 (n=3). Also see table S3.

1278 E) Trehalose levels in *tdh2Δtdh3Δ* cells. WT and *tdh2Δtdh3Δ* cells were grown in high glucose
1279 and trehalose amounts were estimated using targeted LC-MS/MS. Data represent mean ± SD
1280 (n=3).

1281 F) Pi levels in *ubp3Δ* and *tdh2Δtdh3Δ* cells in ethanol medium. WT, *ubp3Δ,* and *tdh2Δtdh3Δ*
1282 cells were grown in ethanol medium and the total Pi levels were estimated. Data represent
1283 mean ± SD (n=3).

1284 The statistical significance was calculated using unpaired-student t-test. *p<0.05, **p<0.01,
1285 ***p<0.001.

1286

1287 **Figure S4:**

1288 A) Lack of vacuolar contamination in mitochondria isolated by immunoprecipitation.
1289 Mitochondria were isolated from WT cells grown in high glucose and the protein levels of
1290 Tom20, Cox2, Idh1 and Vph1 and were measured in cell lysate and immunoprecipitated
1291 mitochondria by western blot.

1292 B) Idh1 levels in *ubp3Δ* cells and WT cells grown in high Pi. WT cells were grown in high
1293 glucose, or high glucose and high Pi medium (10mM Pi) and *ubp3Δ* cells were grown in high

1294 glucose, and the Idh1 protein levels were estimated by western blot. A representative blot
1295 (out of n=3) is shown.

1296 C) Mitochondrial membrane potential in *tdh2Δtdh3Δ* cells. WT, *ubp3Δ,* and *tdh2Δtdh3Δ* cells
1297 were grown in high glucose and the mitochondrial membrane potential was measured. Data
1298 represent mean ± SD (n=3)

1299 D) Pi levels in *ubp3Δ* cells grown in low Pi (1mM Pi) vs WT cells. WT cells were grown in high
1300 glucose and *ubp3Δ* cells were grown in high glucose or high glucose-low Pi, and the total Pi
1301 levels were estimated. Data represent mean ± SD (n=3).

1302 E) Ethanol production in *ubp3Δ* cells grown in a low Pi medium. WT cells were grown in high
1303 glucose and *ubp3Δ* cells were grown in high glucose or high glucose-low Pi, and the ethanol
1304 concentration in the medium was measured. Data represent mean ± SD (n=3).

1305 F) Pi amounts and mitochondrial membrane potential in WT, *ubp3Δ,* and *tdh2Δtdh3Δ* cells.
1306 The cells were grown in high glucose or high glucose-low Pi, and the mitochondrial membrane
1307 potential was measured. Data from two independent experiments (n=2) is shown.

1308 G) The protein levels of mitochondrial Pi transporters Mir1 and Pic2 in *ubp3Δ* cells. WT and
1309 *ubp3Δ* cells containing endogenously tagged Mir1 and Pic2 at their C terminus with a 6x HA
1310 epitope tag were grown in high glucose and Mir1 and Pic2 proteins were measured by
1311 western blot. A representative blot (out of n=3) is shown.

1312 The statistical significance was calculated using unpaired-student t-test. *p<0.05, **p<0.01,
1313 ***p<0.001.

1314

1315 **Figure S5:**

1316 A) Requirement of Mir1 for switching to increased mitochondrial activity upon 2-
1317 deoxyglucose (2-DG) treatment. WT and *mir1Δ* cells were grown in high glucose and treated
1318 with 0.1% and 0.25% 2-DG for one hour. The mitochondrial membrane potential was
1319 measured from two independent experiments (n=2).

1320 B) Mir1 protein levels and glucose repression. Cells containing Mir1 endogenously tagged at
1321 the C terminus with a 6x HA epitope tag were grown in high glucose or a respiratory medium
1322 (2% ethanol). Mir1 protein was estimated by western blot. A representative blot (n=3) is
1323 shown in the panel.

1324 C) Effect of supplementing Pi in the medium on mitochondrial Pi. WT cells were grown in high
1325 glucose, and high glucose, high Pi medium (10 mM Pi), mitochondria was isolated and the
1326 mitochondrial Pi levels were estimated. The mitochondrial Pi levels normalised to Idh1
1327 protein levels is shown. Data represent mean ± SD (n=3). Also see supplementary figure S4B.

1328 D) Increasing the Pi concentration in a high glucose medium results in a decrease in basal OCR.
1329 WT cells were grown in high glucose medium (YPD-Pi medium), supplemented with 5 mM Pi
1330 and at OD_{600}~0.6, the medium was supplemented with Pi (10 mM and 25 mM final
1331 concentrations). The basal OCR was measured one hour after Pi supplementation. Data
1332 represent mean ± SD (n=3).

1333 E) Effect of increasing the Pi concentration in a high glucose medium, in the presence of a
1334 glycolytic inhibitor, on basal OCR. WT cells were grown in high glucose medium (YPD-Pi
1335 medium), supplemented with 5 mM Pi and at OD_{600}~0.6, the medium was supplemented with
1336 Pi (25 mM final concentration) and 2DG (0.25%) for one hour and the basal OCR was
1337 measured. Data represent mean ± SD (n=3).

1338 F) Overexpression of Mir1 under the G6PD promoter. C terminal 6x HA epitope-tagged Mir1
1339 was expressed under G6PD promoter in cells with Mir1 endogenously tagged at the C
1340 terminus with a 6x HA epitope tag. WT cells (carrying an empty vector, and expressing Mir1-
1341 HA under the endogenous Mir1 promoter) and Mir1-OE cells were grown in high glucose. The
1342 protein levels of Mir1 were estimated by western blot, and clones with an ~2 fold increase in
1343 Mir1 were selected. A representative blot (n=3) is shown.

1344 G) Mpc3 protein levels in *ubp3Δ* cells. WT and *ubp3Δ* cells containing endogenously tagged
1345 Mpc3 at the C terminus with a 3x FLAG epitope tag, were cultured in high glucose (2% glucose)
1346 and high glucose-low Pi (2% glucose, 1 mM Pi). The Mpc3 protein levels were measured by
1347 western blot. A representative blot (n=3) is shown in the panel.

1348 H) Mpc3 protein amounts upon shifting WT and *mir1Δ* cells to a low-glucose medium. WT and
1349 *mir1Δ* cells containing Mpc3-FLAG, were cultured in high glucose (2% glucose) and shifted to
1350 low (0.1%) glucose for 1 hour. Mpc3 protein was measured by western blot. A representative
1351 blot (n=3) is shown in the panel.

1352 I) Requirement of Mpc3 for the increase in basal OCR upon shifting to low glucose. WT and
1353 *mpc3Δ* cells were cultured in high glucose (2% glucose) and shifted to low (0.1%) glucose for
1354 1 hour. The basal OCR from two independent experiments (n=2), normalized to the OD_{600} is
1355 shown.

1356 J) Mpc3 protein levels and Mir1 overexpression. WT cells and Mir1-OE cells containing
1357 endogenously tagged Mpc3 ate the C terminus with a 3x FLAG tag were grown in high glucose.
1358 The protein levels of Mpc3 were estimated by western blot. A representative blot (n=3) is
1359 shown in the panel.

1360 The statistical significance was calculated using unpaired-student t-test. *$p<0.05$, **$p<0.01$,
1361 ***$p<0.001$.

Figure 1: A deubiquitinase deletion screen identifies Ubp3 as a regulator of glucose-mediated mitochondrial repression

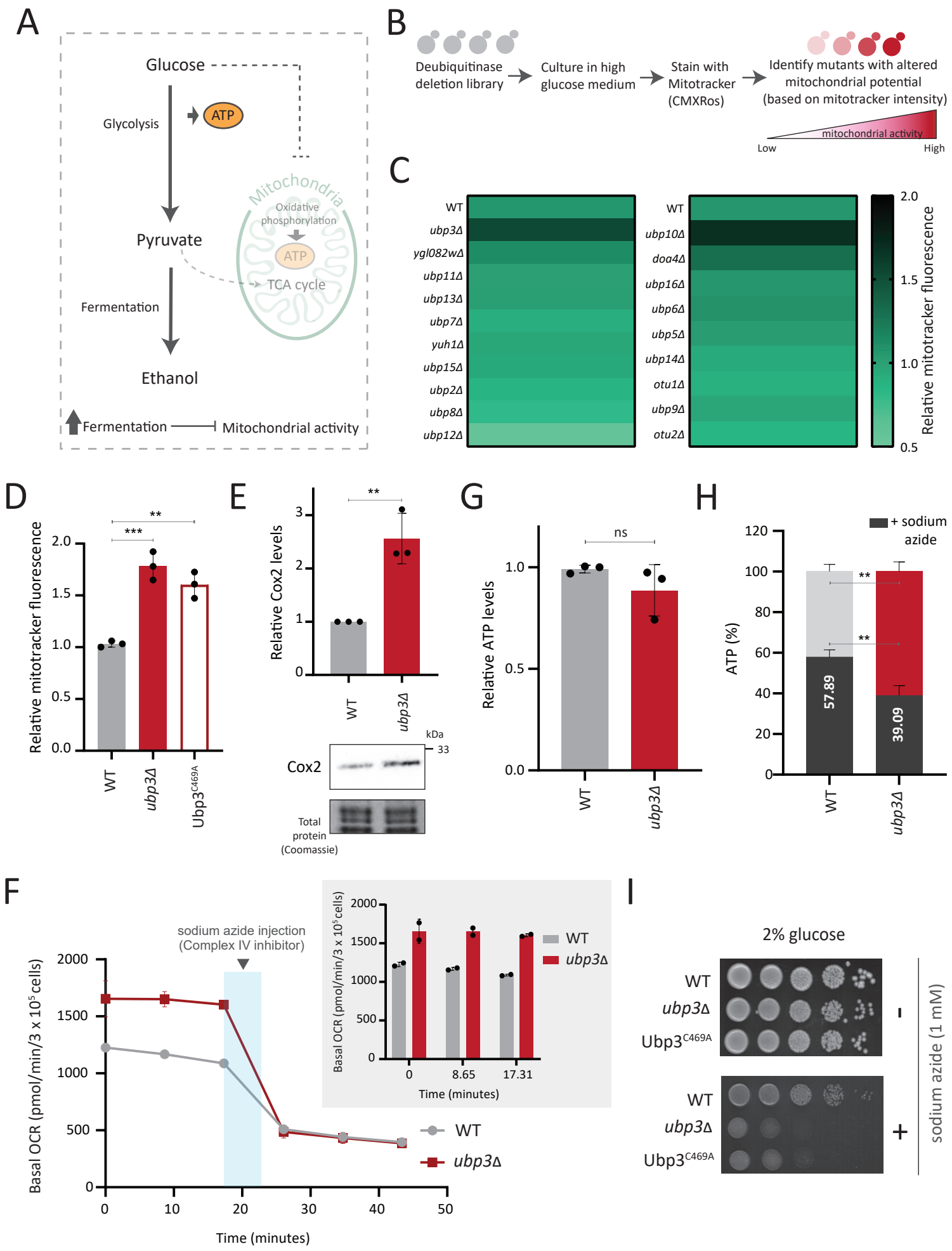

Figure 2: Key glycolytic enzymes decrease and glucose flux is rerouted in *ubp3Δ* cells

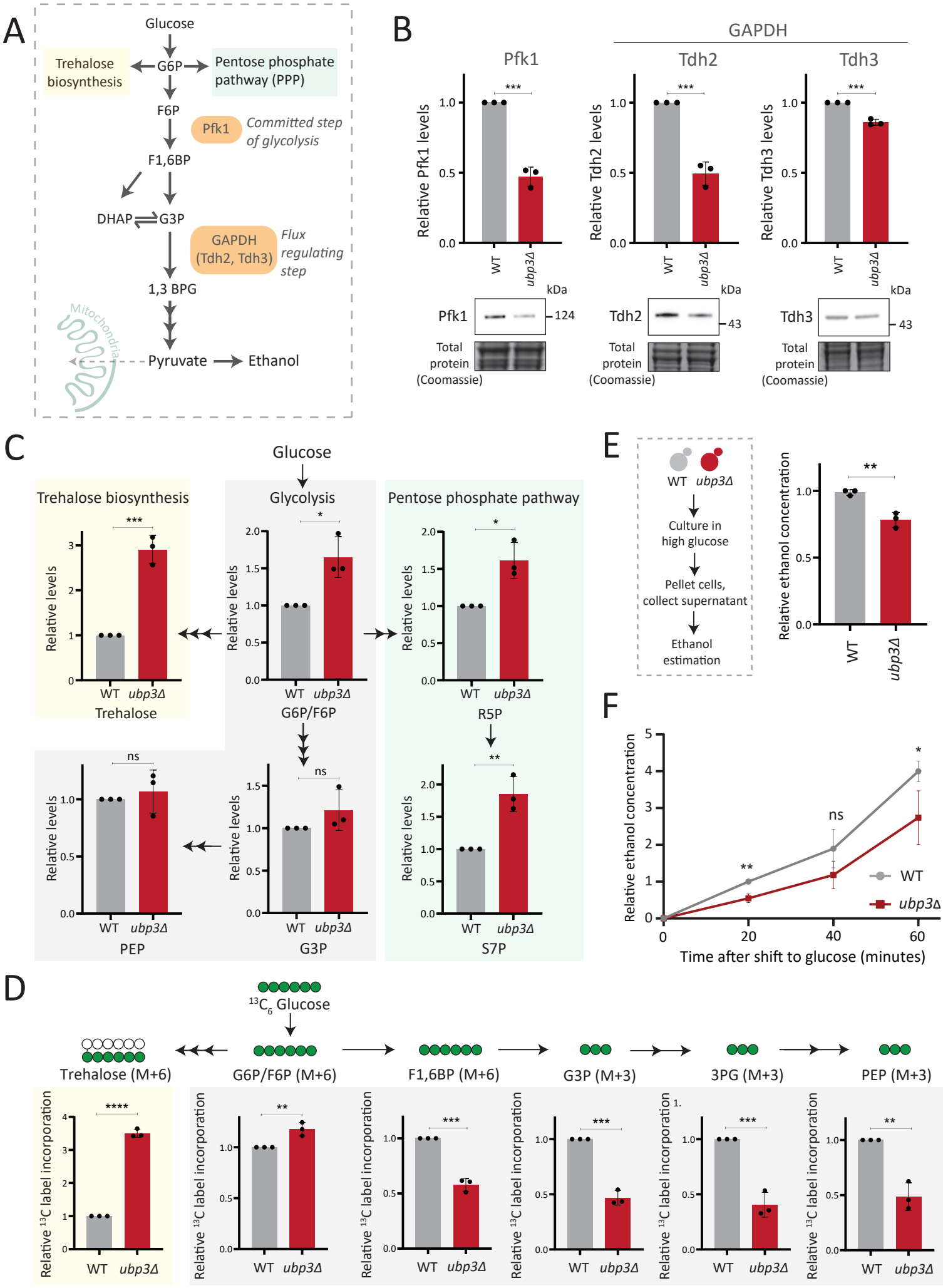

Figure 3: Phosphate accumulates due to altered Pi homeostasis in *ubp3Δ* cells

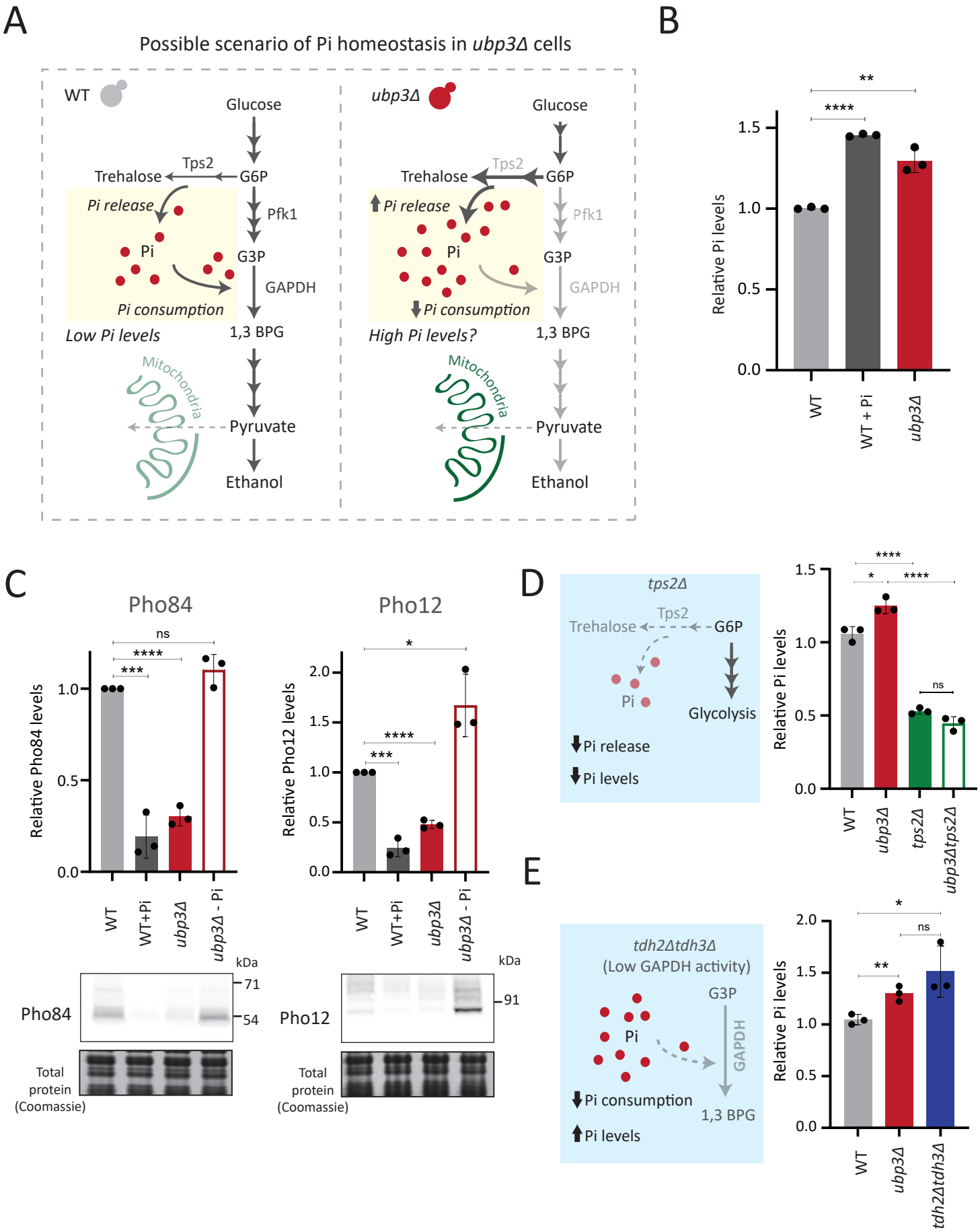

Figure 4: Phosphate availability dictates mitochondrial activity

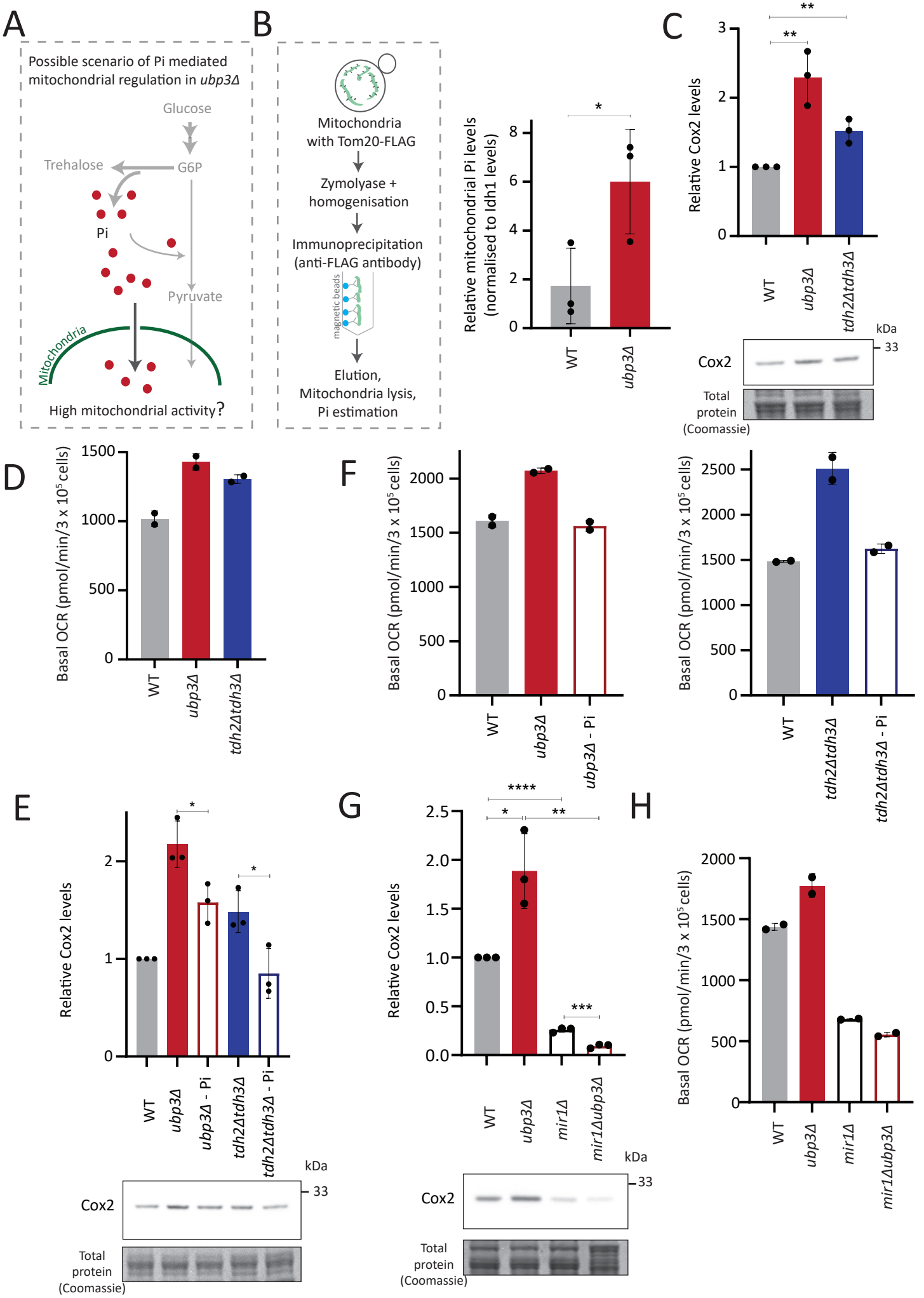
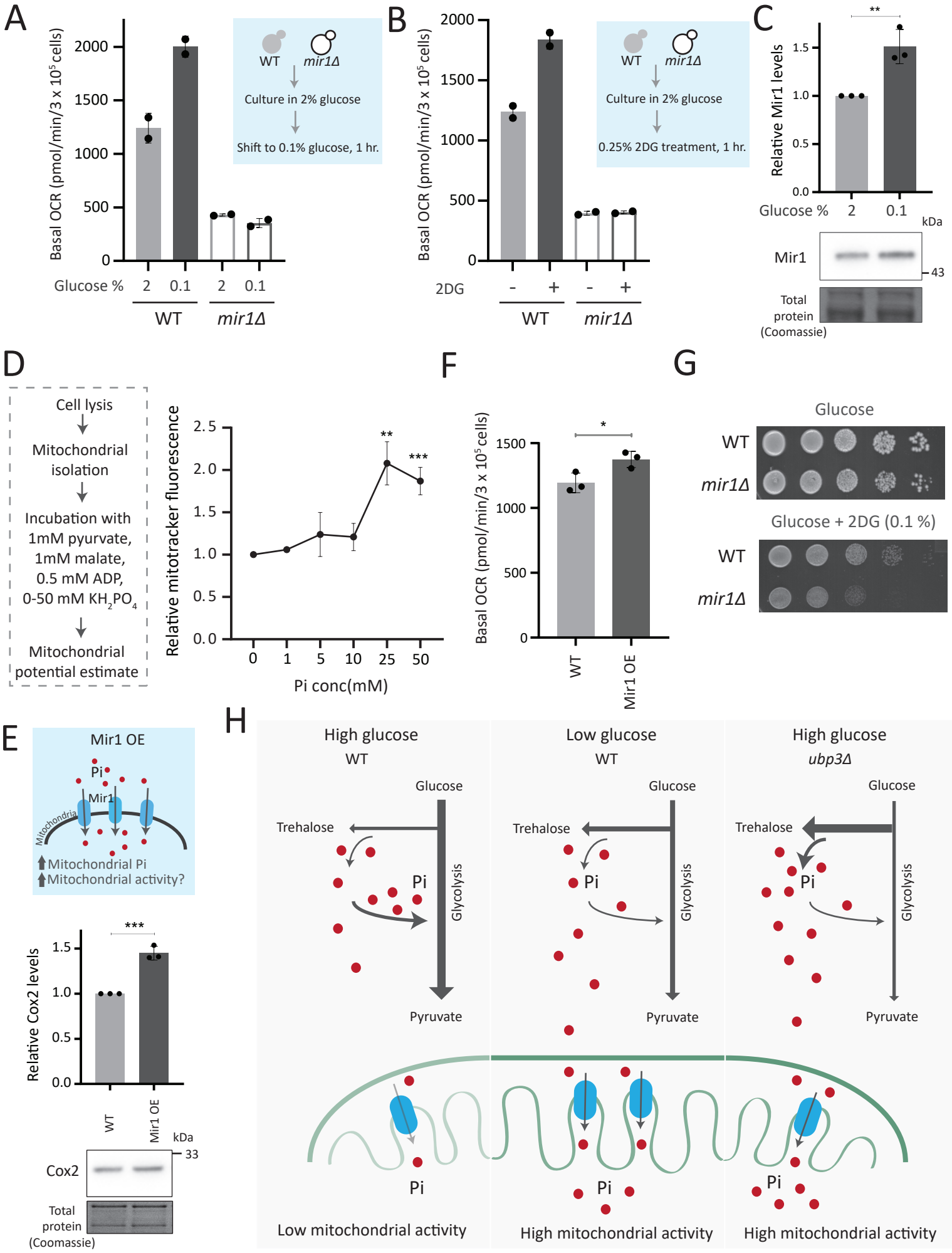
Figure 5: Mitochondrial Pi availability controls glucose-mediated mitochondrial repression